Journal of Medicinal Chemistry

pubs.acs.org/jmc

Article

Selective Pseudo-irreversible Butyrylcholinesterase Inhibitors Transferring Antioxidant Moieties to the Enzyme Show Pronounced Neuroprotective Efficacy In Vitro and In Vivo in an Alzheimer's Disease Mouse Model

Matthias Scheiner, Matthias Hoffmann, Feng He, Eleonora Poeta, Arnaud Chatonnet, Barbara Monti, Tangui Maurice, and Michael Decker*

Cite This: *J. Med. Chem.* 2021, 64, 9302−9320

Read Online

ACCESS | Metrics & More | Article Recommendations | Supporting Information

ABSTRACT: A series of multitarget-directed ligands (MTDLs) was designed by functionalizing a pseudo-irreversible butyrylcholinesterase (BChE) inhibitor. The obtained hybrids were investigated in vitro regarding their *h*BChE and *h*AChE inhibition, their enzyme kinetics, and their antioxidant physicochemical properties (DPPH, ORAC, metal chelating). In addition, in vitro assays were applied to investigate antioxidant effects using murine hippocampal HT22 cells and immunomodulatory effects on the murine microglial N9 cell line. The MTDLs retained their antioxidative properties compared to the parent antioxidant-moieties in vitro and the inhibition of *h*BChE was maintained in the submicromolar range. Representative compounds were tested in a pharmacological Alzheimer's disease (AD) mouse model and demonstrated very high efficacy at doses as low as 0.1 mg/kg. The most promising compound was also tested in BChE$^{-/-}$ mice and showed reduced efficacy. In vivo neuroprotection by BChE inhibition can be effectively enhanced by incorporation of structurally diverse antioxidant moieties.

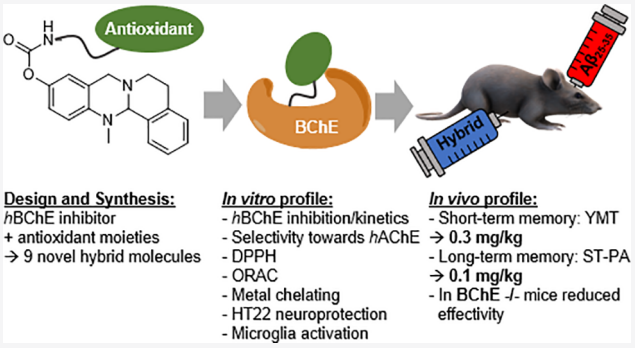

INTRODUCTION

While an estimated number of 50 million people suffered from dementia in 2019 and an increasing number of patients is forecasted, no breakthroughs in the therapy of the disease could be achieved in the past decades.[1] For the treatment of the most common form of dementia, Alzheimer's disease (AD), only four drugs are currently approved, acting purely symptomatic at early disease stages.[2] AD is associated with a loss of the neurotransmitter acetylcholine (ACh) causing dementia symptoms and leading to the oldest theory about AD, the cholinergic hypothesis.[3−5] Three of the drugs (galantamine, rivastigmine, and donepezil) are based on this hypothesis. To counteract AD-caused memory decline, these drugs are inhibiting the ACh hydrolyzing enzyme acetylcholinesterase (AChE) and, therefore, increase the level of ACh in the central nervous system (CNS) but also in the periphery.[2] The latter causes unwanted side effects and can prevent patients from achieving effective doses of the drug.[6] Under healthy conditions, the hydrolysis of ACh is mainly catalyzed by AChE. However, in advanced AD, the ratio of ACh hydrolysis is shifted toward hydrolysis mediated through butyrylcholinesterase (BChE).[7−9] This shift was also observed in homozygous AChE knock out (AChE$^{-/-}$) mice, which did not suffer from cholinergic hyperactivation since BChE can take over the role of AChE.[10] But more importantly, we have recently demonstrated, that chronic administration of a very potent and selective carbamate-based BChE inhibitor in an AD mouse model caused neuroprotection and led to pronounced improvement of both short- and long-term memory deficits.[11] Furthermore, BChE invalidation (using BChE$^{-/-}$ mice) or inhibition (using pharmacological inhibitor) is associated with beneficial effects and neuroprotection in several AD in vivo models.[11−14] Taking this into account, BChE represents a promising target for later stages of AD. However, AD drug candidates in clinical trials of the past decades, following the "one drug−one target−one disease" dogma showed no positive outcome.[15] This might be due to the multifactorial nature and complex pathophysiology of AD. Consequently, the multitarget directed ligand (MTDL) approach, that is, addressing several targets with only one drug, has become the focus of AD research.[16,17] Following this approach, GV-971 has been

Received: March 23, 2021
Published: June 21, 2021

approved in China for the treatment of AD.[18,19] GV-971 is indirectly modifying microglia cells and, thus, addresses another hallmark of AD, neuroinflammation.[19,20] Microglia represent the CNS immune system and can display two activation phenotypes: the pro-inflammatory (M1) and the neuroprotective (M2) phenotype. In the case of AD, microglia are activated by soluble amyloid β (Aβ), Aβ oligomers and fibrils or neurofibrillary tangles, as well as by other factors secreted by damaged neurons.[20,21] In early stages of AD, the neuroprotective M2 phenotype is predominant and can promote Aβ clearance, while in later stages, the phenotype switches to the M1. The latter is characterized by the release of proinflammatory cytokines and chemokines, which are associated with neuronal damage and, ultimately, the progression of AD.[21] Another characteristic of AD is oxidative stress.[22] Neurodegeneration is also due to formation of reactive oxygen species (ROS) caused inter alia by a disbalance in metal ion homeostasis. It was shown that redox-active metal ions form ROS directly or bound in a complex with Aβ.[22,23]

Our group recently reported a series of tetrahydroisoquinazoline-based selective pseudo-irreversible *h*BChE-inhibitors.[11,24,25] The inhibition mechanism of the carbamate is based on a pseudo-irreversible inhibition mechanism of *h*BChE and can therefore be divided into different steps (cf., Figure 1 and Figure 2). In a first step, a reversible complex (EC−X) between the enzyme (E) and the carbamate (C−X) is formed. The formation of (EC−X) is characterized by k_1 and its dissociation by k_2. The K_c-value describes an overview of this reversible process. The reversible complex (EC−X) can form a stable complex by carbamylation of the catalytic active Ser198 resulting in cleavage of the leaving group (X). This step is characterized by the kinetic parameter k_3. However, the formed complex E−C is pseudo-irreversible and only stable for certain period. Since the carbamylated Ser198 is hydrolyzed off the enzyme under release of the carbamate (C), the enzyme regains its activity. The duration of the carbamylated state E−C is characterized by k_4 (cf., Figure 1). In the previously described series of BChE inhibitors, we followed an approach improving the efficacy by improving the inhibitory potency on solely *h*BChE. Recently, we were able to show that the duration of the inhibitor can be extended depending on the moiety transferred to *h*BChE. Remarkably, the extent and duration of enzyme inhibition not only had the desired in vitro effect, but the compounds also showed pronounced effects on preventing cognitive decline in an AD mouse model. Prolonged inhibition by chemical modification was more effective in vivo.[11]

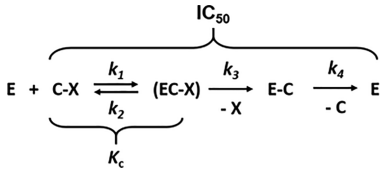

Figure 1. Kinetic parameters of pseudo-irreversible inhibition of an enzyme (E) by a carbamate (C−X) containing a leaving group (X).

DESIGN

We started our compound design by choosing the selective carbamate-based *h*BChE inhibitor scaffold **1**. The *h*BChE inhibitor **1** consists of two components: (i) the part of the carbamate which is transferred to the catalytically active Ser198 of *h*BChE and is, therefore, mainly responsible for the duration of action in case of an additional interaction with an allosteric side[11] and (ii) the part also referred to as "carrier" **2**, on which the high selectivity over *h*AChE is based (cf., Figure 2).[24,25] In our previous work, direct attachment of bulky residues to the carrier part decreased, while attachment via a longer alkylene linker increased half-life time of carbamylated *h*BChE.[11] Therefore, the concept of hybridization was used for the design of novel MTDLs, which is based on the connection of two drugs via a linker.[26] In our case the replacement of a cyclic structure in the transferred unit by a suitable antioxidant leads to incorporation into the inhibitor, without significantly increased pharmacokinetically relevant parameters like molar mass. Therefore, both the carbamate itself and its hydrolysis product have an antioxidant effect. Similar concepts have been followed in the past, in which active compounds, that is, inhibitors or receptor ligands are released after the hydrolysis of the carbamate based-inhibitor by an targeted enzyme.[27,28] Also reversible, selective and unselective BChE inhibitors, with

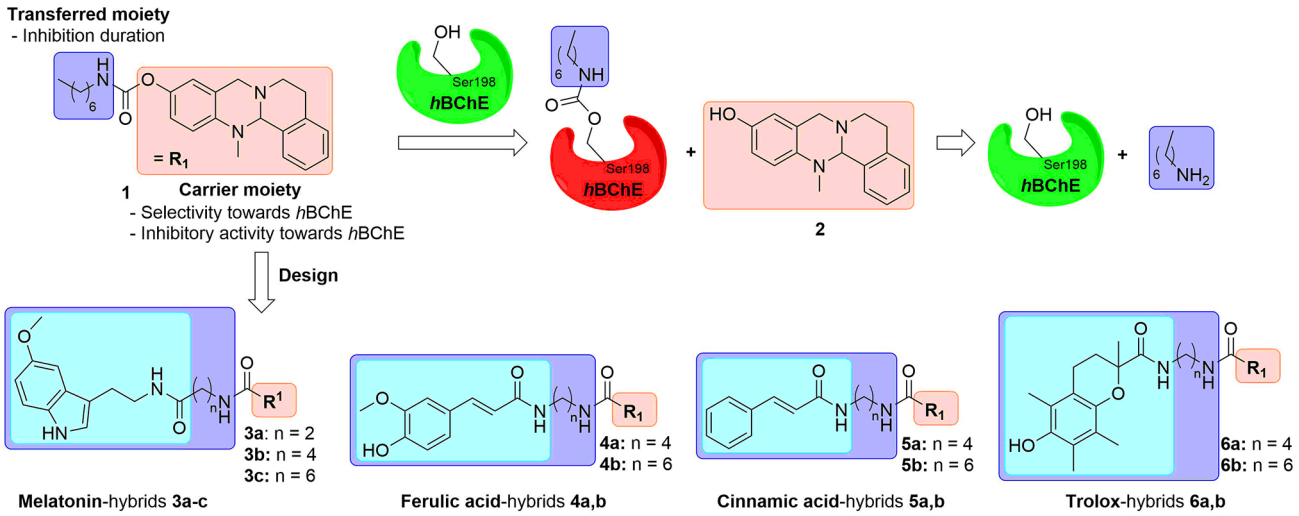

Figure 2. Lead structure of carbamate based selective *h*BChE inhibitor **1**,[11,25,46] its mode of *h*BChE inhibition and release of the phenolic tetracyclic carrier **2**, and designed MTDL **3a−c**, **4a,b**, **5a,b**, and **6a,b**.

https://doi.org/10.1021/acs.jmedchem.1c00534
J. Med. Chem. 2021, 64, 9302−9320

Scheme 1. Synthesis of Melatonin Hybrids 3a−c[a]

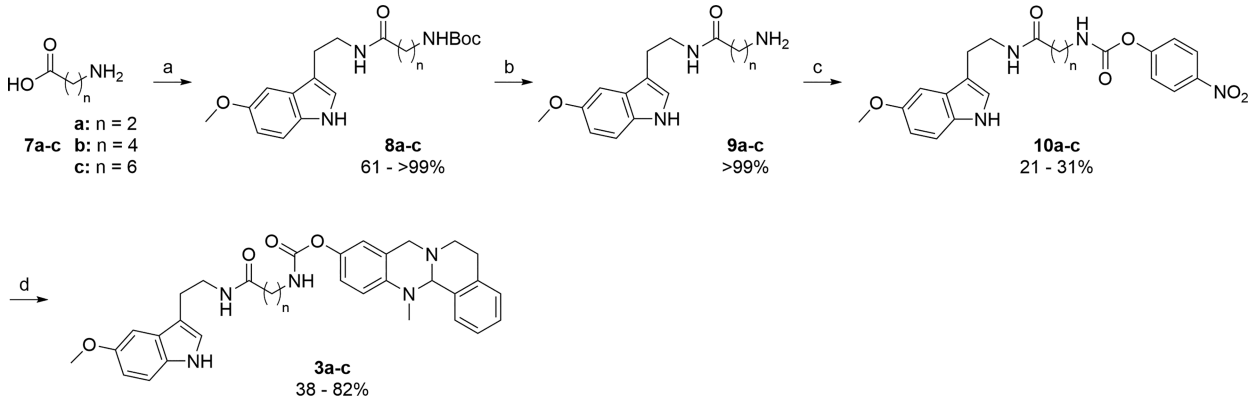

[a]Reagents and conditions: (a) (1) Boc_2O, NEt_3, DMF, (2) 2-(5-methoxy-1*H*-indol-3-yl)ethan-1-amine, HBTU; (b) 5% TFA in CH_2Cl_2; (c) 4-nitrophenyl chloroformate, NEt_3, dry CH_2Cl_2; (d) **2**,[11,25,47] NaH, dry CH_2Cl_2.

Scheme 2. Synthesis of Ferulic Acid Hybrids 4a,b, Cinnamic Acid Hybrids 5a,b, and Trolox Acid Hybrids 6a,b

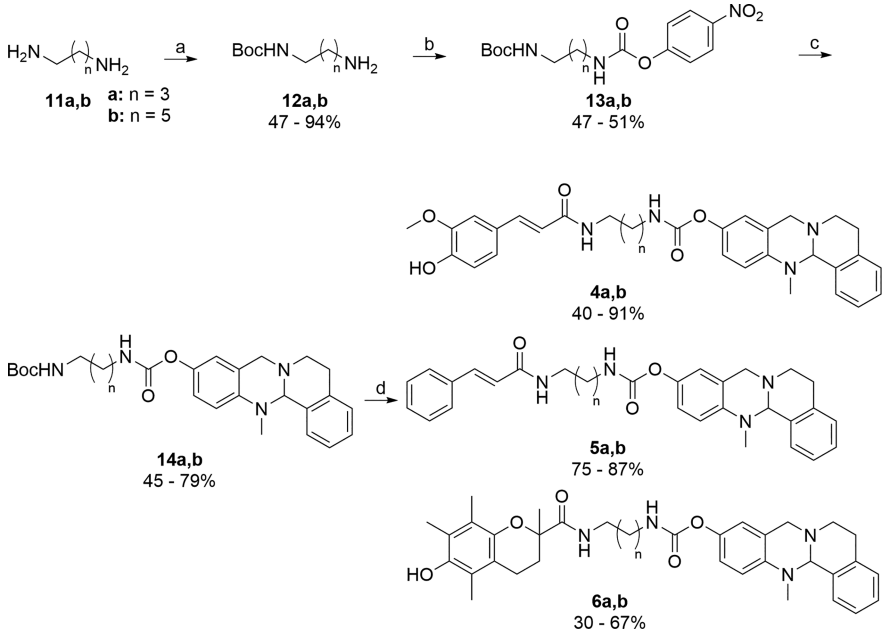

[a]Reagents and conditions: (a) Boc_2O, NEt_3, CH_2Cl_2; (b) 4-nitrophenyl chloroformate, NEt_3, dry CH_2Cl_2; (c) **2**,[11,25,47] NaH, dry CH_2Cl_2; (d) (1) 2 M HCl in MeOH, (2) respective antioxidant moiety (i.e., ferulic acid, cinnamic acid, Trolox), HBTU, NEt_3, DMF.

antioxidative properties are described.[30−32] In our case, an antioxidative motive is released over the time in an environment probably affected in case of AD.[33−35] To retain selectivity and high inhibitory activity of **1** toward *h*BChE, the antioxidant moieties were incorporated at the amine side. Various antioxidants that are suitable for the MTDL approach are described in the literature.[36,37] In this work, melatonin (derivatives **3a−c**),[38,39] ferulic acid (derivatives **4a,b**),[40,41] cinnamic acid (derivatives **5a,b**),[42,43] and Trolox (derivatives **6a,b**)[44,45] were selected as antioxidant moieties (cf., Figure 2).

RESULTS AND DISCUSSION

Chemistry. For the synthesis of melatonin hybrids **3a−c**, the amine moiety of the respective *ω*-amino acids **7a−c** was protected by reacting with Boc_2O, followed by direct coupling of the acid to commercially available 2-(5-methoxy-1*H*-indol-3-yl)ethan-1-amine by amide formation using HBTU. The resulting amides **8a−c** were deprotected using TFA. In the next step, amines **9a−c** were activated using 4-nitrophenyl chloroformate and activated carbamates **10a−c** were directly transferred to the tetracyclic phenolate **2**, which had been synthesized as previously described, to obtain melatonin hybrids **3a−c**.[11,25,47]

Hybrid molecules **4a,b**, **5a,b**, and **6a,b** were synthesized following a synthetic strategy using last-step derivatization. Therefore, precursors **14a,b** were synthesized starting with the monoprotection of the respective diamines **11a,b** by reaction with Boc_2O. Monoprotected amines **12a,b** were activated to **13a,b** using 4-nitrophenyl chloroformate and directly transferred to the deprotonated tetrahydroisoquinazoline-based carrier scaffold **2** to form carbamates **14a,b**. The selective hydrolysis of the protection group to obtain the primary amine was achieved with 2 M HCl in MeOH. The deprotected amines were not stable inter alia because of the formation of urea derivatives. Therefore, deprotection was directly followed by amide coupling in one step. Amide formation to hybrids

https://doi.org/10.1021/acs.jmedchem.1c00534
J. Med. Chem. 2021, 64, 9302−9320

Table 1. Results of the In Vitro Evaluation of the Inhibitory Effect on *h*AChE/*h*BChE and Antioxidative Properties in ORAC and DPPH-Assay of Hybrids 3a−c, 4a,b, 5a,b, and 6a,b, Respectively[d]

	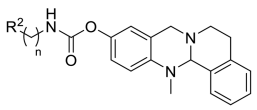 R²	n	IC_{50} *h*BChE [nM] (pIC_{50} ± SEM)[a]	IC_{50} *h*AChE [nM] (pIC_{50} ± SEM) or Inhibition of *h*AChE ± SEM@ 10 μM[b]	$t_{1/2}$ (E-C) [h] ± SD[a]	ORAC equiv.[c]	IC_{50} DPPH-assay [μM] (pIC_{50} ± SEM)
Ascorbic acid			n.d.	n.d.	n.d.	n.d.	11.5
Melatonin			n.a	n.a.	n.d.	2.60 ± 0.12	n.a.
Ferulic acid			n.a	n.a	n.d.	3.15 ± 0.22	14.2
Cinnamic acid			n.a	n.a.	n.d.	n.a.	n.a.
Trolox			n.a	n.a	n.d.	1,05 ± 0.10	8.6
Tacrine			54.0 (7.37 ± 0.02)	111 (6.96 ± 0.02)	n.d.	n.d.	n.d.
1		6	6.4[46] (8.19 ± 0.02)	3800[46] (5.42 ± 0.05)	1.12[46]	0.3 ± 0.12[25]	n.d.
3a	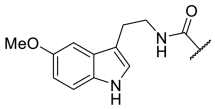	2	482 (6.32 ± 0.03)	2.3% ± 5.3	n.d.	2.80 ± 0.31	n.a.
3b	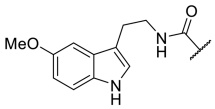	4	127 (6.90 ± 0.01)	15% ± 1.2	n.d.	2.61 ± 0.35	n.a.
3c	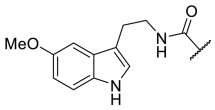	6	102 (6.69 ± 0.02)	6.5% ± 1.8	3.00 ± 0.26	2.20 ± 0.24	n.a.
4a	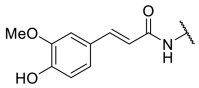	4	155 (6.94 ± 0.02)	7.7% ± 1.5	2.40 ± 0.09	2.63 ± 0.42	14.2 (4.85 ± 0.01)
4b	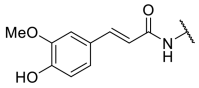	6	166 (6.78 ± 0.02)	20% ± 0.9	n.d.	2.19 ± 0.40	13.6 (4.87 ± 0.02)
5a	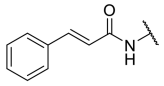	4	221 (6.66 ± 0.03)	6.1% ± 2.7	n.d.	1.65 ± 0.37	n.a.
5b	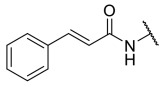	6	442 (6.35 ± 0.04)	37.5% ± 0.5	n.d.	1.83 ± 0.50	n.a.
6a	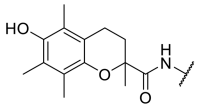	4	791 (6.10 ± 0.05)	15.2% ± 0.6	n.d.	3.15 ± 0.33	8.1 (5.09 ± 0.02)
6b	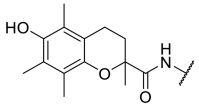	6	255 (5.03 ± 0.2)	24.1% ± 1.3	n.d.	2.38 ± 0.27	9.3 (5.03 ± 0.02)

[a]Values are the mean of at least three determinations. *h*BChE from human serum. [b]Values are the mean of at least three determinations. *h*AChE recombinant expressed. [c]Data are expressed as μmol of Trolox equivalents/μmol of tested compound of at least four determinations. [d]n.d. = not determined. n.a. = not active at highest tested concentration (50 μM in DPPH, 4 μM in ORAC, 10 μM in ChE assays).

https://doi.org/10.1021/acs.jmedchem.1c00534
J. Med. Chem. 2021, 64, 9302−9320

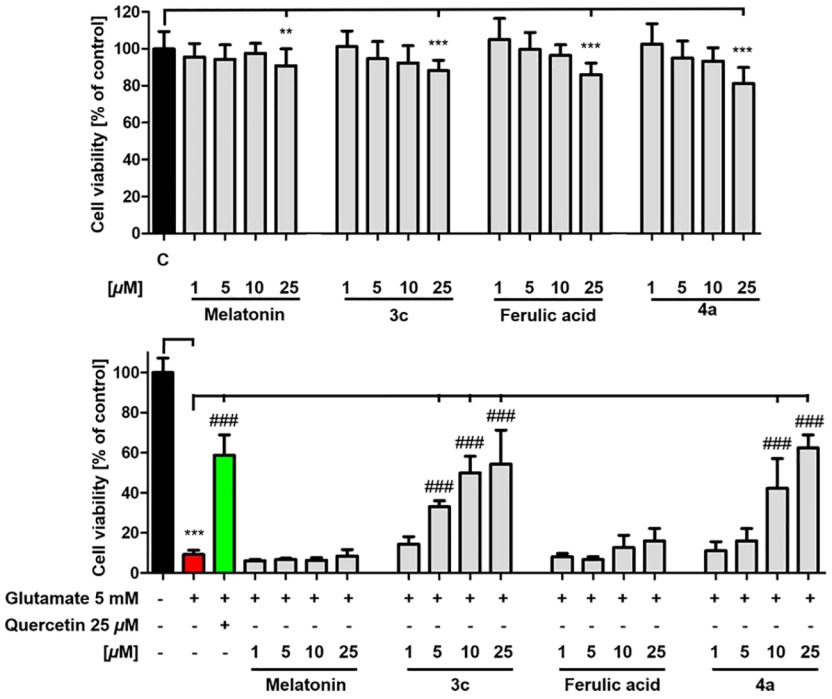

Figure 3. Parent antioxidative moieties melatonin and ferulic acid, as well as respective hybrids **3c**, and **4a**, were studied for neurotoxic effects (upper panel) and neuroprotection against glutamate induced oxidative stress at 1−25 μM (lower panel). Results of the modified MTT tests are presented as means ± SEM of three independent experiments, each performed in sextuplicate and refer to untreated control cells which were set as 100% values. Statistical analysis was achieved by applying one-way ANOVA followed by Dunnett's multiple comparison post-test. Levels of significance: $^{*}p < 0.05$, $^{**}p < 0.01$, $^{***}p < 0.001$, $^{\#}p < 0.05$, $^{\#\#}p < 0.01$, $^{\#\#\#}p < 0.001$.

4a,b, **5a,b**, and **6a,b** was performed using HBTU and the acids of the respective antioxidant moieties.

Enzyme Inhibition. All hybrids were tested for ChE inhibition using a modified colorimetric Ellman's assay.[24,48,49] To determine the IC_{50}-values, the hybrid was incubated with the respective human ChE for 20 min.[11,50] Since all the kinetic steps described above are taking place simultaneously during these 20 min of incubation, the IC_{50}-value represents a summative parameter only (cf., Figure 1). All hybrids retained excellent selectivity over *h*AChE. Except for ferulic acid hybrids **4a,b**, linker length has an significant influence on inhibitory potency of the hybrids in terms of the IC_{50}-values.[24,25] While the inhibitory potency increased with increasing linker length for melatonin- (**3a−c**), and Trolox-hybrids(**6a,b**), the opposite trend was observed for cinnamic acid hybrids (**5a,b**). Although hybrids have in common that they have lost inhibitory potency in comparison to the lead structure **1** but still represent potent inhibitors. Hybrids **3c** and **4a** represent the most promising compounds in terms of *h*BChE inhibition and were, therefore, further characterized and the stability of *h*BChE carbamylation was investigated. The *h*BChE was, therefore, incubated with a high concentration of the inhibitor, followed by a strong dilution (1000×), so that ultimately only decarbamylation can take place. The *h*BChE activity of the diluted solution was assessed at various time points and increasing activity over time observed. Both hybrids tested showed extended duration of action in terms of residence time, whereas hybrid **3c** almost tripled the half-life time of the carbamylated *h*BChE compared to lead structure **1**. According to our previous study, incorporation of an electron rich aromatic moieties to the amine side of the inhibitor resulted in a prolonged duration of inhibition, due to interactions with the PAS.[11] It can, therefore, be assumed that the antioxidant motifs interact with the PAS and thus extend the half-life.

Physicochemical Antioxidant Activities. Antioxidants can be divided into three groups according to their antioxidative mode of action: electron transfer (ET), hydrogen atom transfer (HAT), and chelation of transition metals, such as Fe^{2+} or Cu^{2+}.[51] In case of ET, the antioxidant can reduce a free radical by an electron transfer, while for HAT the inactivation of the free radical is achieved by donation of hydrogen. As transition metals (especially Fe^{2+} and Cu^{2+}) are involved in the formation of ROS in vivo, chelation leads to reduced production of ROS.[52] All hybrids were studied for their antioxidant properties and the underlying mode of action. To investigate a possible antioxidant effect by ET, the 2,2-diphenyl-1-picrylhydrazyl (DPPH) assay was used. DPPH represents a stable radical. By reacting with a radical scavenger, the absorption maximum changes which enables colorimetric determination of this interaction. Of the parent antioxidative moieties, only ferulic acid and Trolox showed activity, while melatonin and cinnamic acid revealed no activity. The respective ferulic acid hybrids (**4a,b**) and Trolox-hybrids (**6a,b**) retained their ET antioxidative properties compared to the parent antioxidative moieties. Antioxidant behavior based on HAT mechanism was investigated using the ORAC assay. The assay is based on the use of fluorescein as a fluorescent probe and AAPH as a peroxyl radical initiator. The parent antioxidant moieties, except cinnamic acid, showed activity. While the activity of the Trolox hybrids **6a,b** decreased, the ferulic acid and melatonin hybrids, **3a−c** and **4a,b**, respectively, showed a slight improvement. Even the cinnamic acid hybrids **5a,b** showed activity, which is attributed to the activity of the carrier moiety of the BChE inhibitor.[24] A ferrozine and pyrocatechol assay was carried out in order to investigate a

https://doi.org/10.1021/acs.jmedchem.1c00534
J. Med. Chem. 2021, 64, 9302−9320

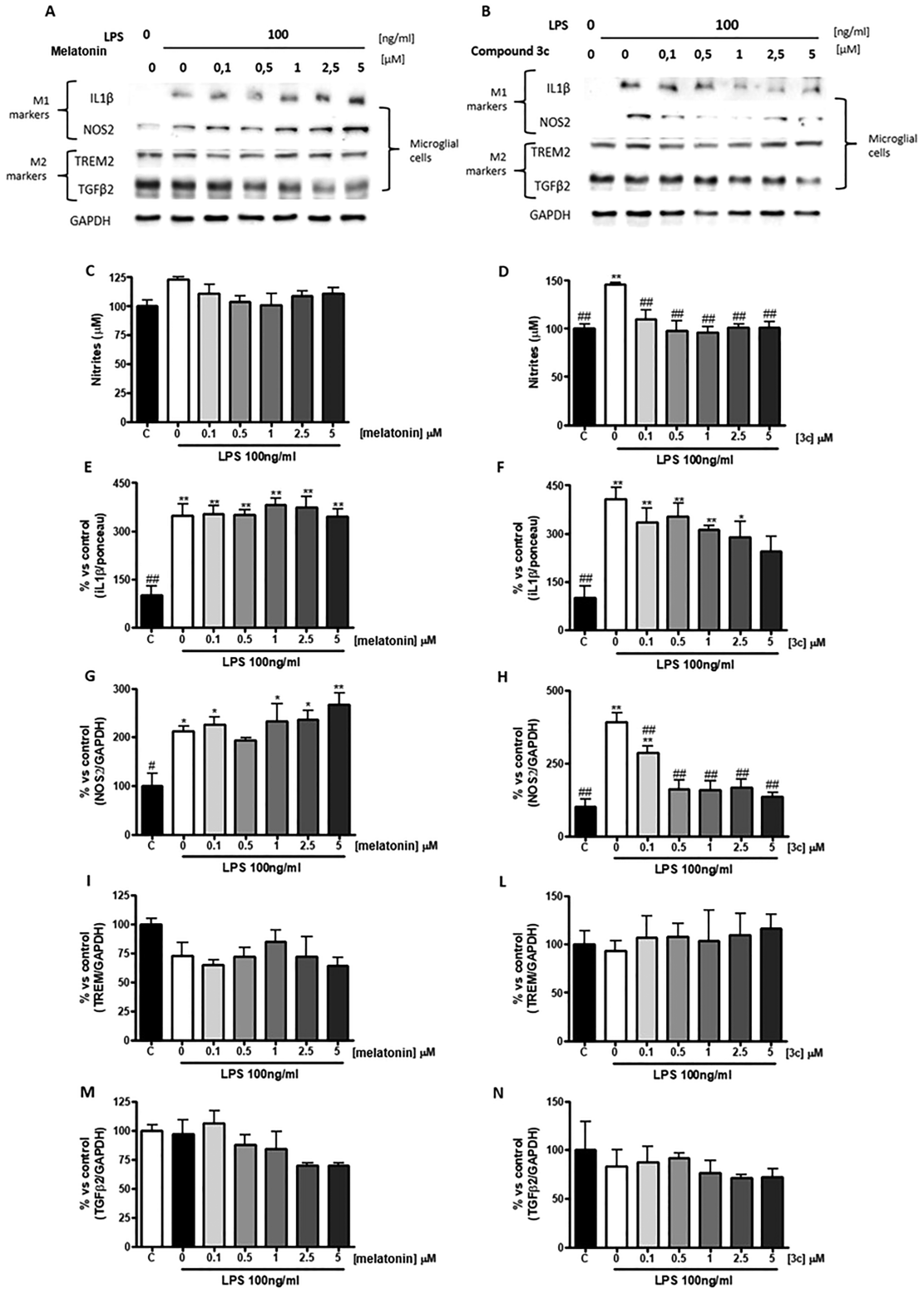

Figure 4. Effect of melatonin and the resulting hybrid **3c** on murine N9 cells, following induction in M1 activation state by LPS (100 ng/mL) treatment. IL1β release and iNOS, TREM2, and TGFβ2 expression were analyzed by Western blot after 24 h treatment with LPS and increasing concentrations (0.1, 0.5, 1, 2.5, and 5 μM) of melatonin (A) and compound **3c** (B). For the indirect determination of nitric oxide (NO) release, nitrites derived from N9-cultured media were quantified through Griess reaction. As shown in Figure 4, hybrid **3c** induced a significant reduction in iNOS expression (H), as well as NO and IL1β release (D, F), compared to LPS-control and the parent antioxidant moiety, whose no effects on microglia activation was observed (C, E, G). Additionally, although no notably differences were observed on TGFβ2 (M, N), TREM2 expression increased in cells cotreated by LPS-**3c** compound (L) compared to melatonin (I), suggesting a potential immunomodulatory effect. Results are presented as means ± SE from 3 independent experiments. Statistical significance was calculated using one-way analysis of variance (ANOVA) and posthoc Bonferroni's comparison test: *p < 0.05; **p < 0.01 compared to untreated control; #p < 0.05; ##p < 0.01 compared to LPS-treated control.

https://doi.org/10.1021/acs.jmedchem.1c00534
J. Med. Chem. 2021, 64, 9302−9320

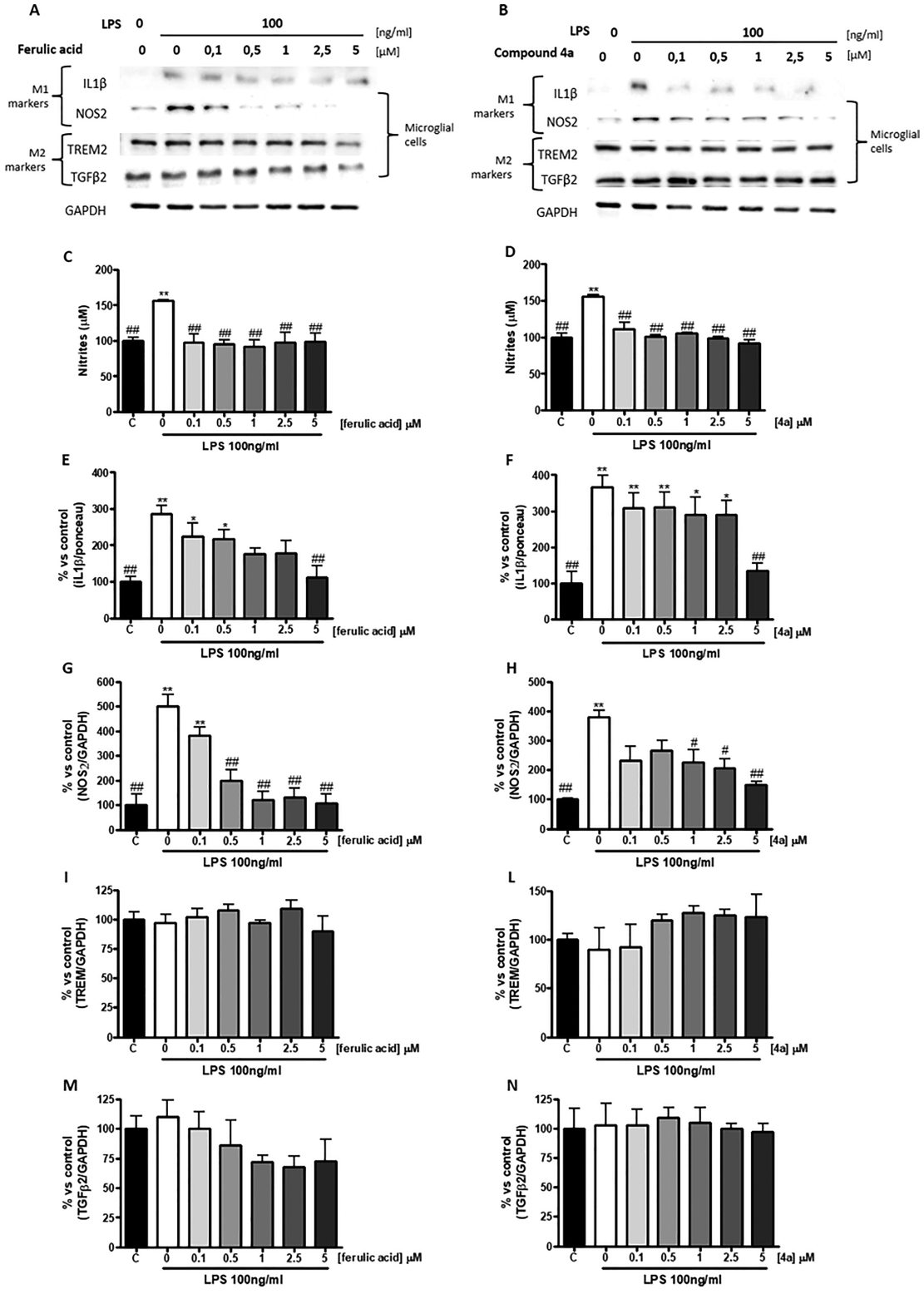

Figure 5. Effect of ferulic acid and the resulting hybrid **4a** on murine N9 cells following induction in M1 activation state by LPS (100 ng/mL) treatment. IL1β release and iNOS, TREM2 and TGFβ2 expression were analyzed by Western blot after 24 h treatment with LPS and increasing concentrations (0.1, 0.5, 1, 2.5, and 5 μM) of ferulic acid (A) and compound **4a** (B). For the indirect determination of Nitric Oxide (NO) release, nitrites derived from N9-cultured media were quantified through Griess reaction. As shown in Figure 5, hybrid **4a** significantly decreased iNOS expression (H), as well as NO and IL1β release (D, F) compared to ferulic acid (C, E, G). Additionally, TREM2 expression (M2 microglia marker) increased in cells treated with compound **4a** compared to LPS-treated control (L) and the parent antioxidant moiety (I). However, no relevant effects were obtained on the expression of the growth factor TGFβ2 (M, N). Results are presented as means ± SE from 3 independent experiments. Statistical significance was calculated using one-way analysis of variance (ANOVA) and posthoc Bonferroni's comparison test: *p < 0.05; **p < 0.01 compared to untreated control; #p < 0.05; ##p < 0.01 compared to LPS-treated control.

https://doi.org/10.1021/acs.jmedchem.1c00534
J. Med. Chem. 2021, 64, 9302−9320

possible chelation of Fe^{2+} and Cu^{2+} by the hybrids. The hybrids were screened at a molar ratio of 10:1 compound to metal ions. As the parent antioxidant moieties did not significantly chelate the transition metals, it is not surprising that the resulting hybrids lack chelating properties (cf., Figure S1). Taken together, the parent antioxidant moieties of **3c** and **4a** and the resulting hybrids differ in their physicochemical antioxidant profile, which is why these hybrids were further investigated.

Neurotoxicity and Neuroprotection on HT22 Cells. The HT22 cell line is glutamate-sensitive because of the lack of the ionotropic glutamate receptor.[53] The addition of high extracellular glutamate concentrations leads to the blocking of the cystine/glutamate antiporter, which is accompanied by glutathione depletion. This causes intracellular accumulation of ROS, which can ultimately lead to cell death.[54−56] Based on the high inhibition of *h*BChE and their different mode of antioxidative actions, hybrids **3c** and **4a**, as well as their parent antioxidant moieties were first tested for possible neurotoxicity on the murine hippocampal neuronal (HT22) cell line. The antioxidant parent moieties, as well as the corresponding hybrids, showed a decrease in cell viability, but no neurotoxic effect even at the highest tested concentration (25 μM) (cf., Figure 3). After ensuring that the tested compounds did not show neurotoxicity, we further investigated their neuroprotective properties on the HT22 cell line and performed a glutamate assay as previously described.[37,57,58] Whereas the parent antioxidant moieties, melatonin and ferulic acid, showed no protective effect at the concentrations applied, while the resulting hybrids **3c** and **4a** showed pronounced protection. Depending on the incorporated antioxidant moiety, a significant effect was observed at 5 μM in case of melatonin hybrid **3c** and 10 μM for the ferulic acid hybrid **4a** (cf., Figure 3)

Effects on Microglia Activation. Neurodegenerative diseases, including AD, are accompanied by neuroinflammation, represented by activation of microglia cells, immune cells of CNS. As previously described, depending on AD progression, in early stages of degeneration microglia show the neuroprotective M2 phenotype, characterized by expression of growth factors, such as TGFβ2, and the phagocytic protein TREM2; subsequently, in later stages of disease, microglia switch to neurotoxic M1, generally distinguished by production of nitric oxide (NO) due to iNOS induction and release of proinflammatory cytokines, likely TNF-α and IL-1β. To analyze the immunomodulatory activity (i.e., the ability to modify microglia cells from the neurotoxic M1 to the neuroprotective M2 phenotype) of the antioxidant moieties, melatonin and ferulic acid, and the resulting hybrids **3c** and **4a**, N9 microglial cells were treated with increasing concentration of these molecules (0.1, 0.5, 1, 2.5, 5 μM), a range coherent with the physiological nature of melatonin, in presence or absence of 100 ng/mL lipopolysaccharide (LPS), which induces M1 activation. After 24 h of treatment, microglial cells were collected, and the expression of the inducible nitric oxide synthase (iNOS; M1 marker), TREM2, and TGFβ2 (M2 markers) was analyzed by Western Blot. In parallel, conditioned media were collected and NO release in microglial cell culture supernatants was spectrophotometrically detected by measuring nitrite accumulation in the medium using the Griess reaction, as well as IL1β release (M1 microglia markers) was evaluated by Western Blot analysis. As shown in Figures 4 and 5, compared to the parent antioxidant moieties (C, E, G) where no relevant (Ferulic acid) or, conversely, potential neurotoxic effects (melatonin) were observed in the presence of high concentration of compound (2.5, 5 μM), the hybrids **3c** and **4a** significantly decreased IL1β release (F) and iNOS expression (H) induced by LPS-mediated microglia activation, and reduced nitrites accumulation (D). More specifically, 3c determines a dose-dependent decrease of ILβ release from 0.5 to 5.0 μM (Figure 4B, F), while compound 4a reduces ILβ release at all concentrations tested, with a stronger effect at 5.0 μM (Figure 5B, F). In addition, compound **3c** and **4a** showed an increase in phagocytic protein TREM2 expression (L) compared to LPS-treated control and the antioxidative moieties (I) at 2.5 and 5 μM, suggesting a potential immunomodulatory effect on microglia and, therefore, a switch from the neurotoxic M1 to the neuroprotective M2 phenotype, at higher concentrations.

In Vivo Neuroprotection Studies. Hybrids **3a−c** and **4a,b** were consequently further investigated in an in vivo AD mouse model leading rapidly to cognitive impairments. To induce the deficits, oligomerized Aβ_{25-35} or vehicle (V1: *dd*H_2O) was intracerebroventricularly (ICV) injected into the mouse brain on day one.[59] On the same day, 20 min after the ICV injection, either test substance or vehicle solution (V2: water/DMSO 1:1) was administered via intraperitoneal (IP) injection. The test substance or V2 was then administered o.d. between day two to seven. Spatial working memory was assessed on day eight using the Y-maze test by measuring the mouse ability to spontaneously alternate during maze exploration. Long-term contextual memory was assessed using the step-through type passive avoidance task, by training animals on day nine and measuring retention on day ten (cf., Figure S2).[12,59,60] Neither the acute ICV injections nor chronic IP injections of vehicle or compounds **3c** or **4a** over 7 days resulted in significant change in the daily weight gain or the natural behavior, which indicates good compound and vehicle solution tolerability (cf., Figure S3). Aβ_{25-35} induced significant learning deficits in both behavioral tests, as compared to V1-treated mice. In the Y-maze test, treatment with compound **3c**, as well as **4a**, showed significant increase in alternation performance compared to Aβ_{25-35}/V2-treated mice, while no significant change in the number of arm entries was observed (cf., Figures 6A, 6B and S4). The melatonin-hybrid **3c** showed a significant protection at 0.3 and 1 mg/kg doses, while the ferulic acid hybrid **4a** showed a significant effect at 1 mg/kg (cf., Figure 6A, 6B). In the passive avoidance test, both compounds significantly prevented the learning deficits at the lowest tested dose, namely, 0.1 mg/kg for **3c** and 0.3 mg/kg for **4a** (cf., Figure 6C, 6D). It should be noted that the hybrids show a significantly higher in vivo efficacy compared to the parent BChE-inhibitor **1**, which was tested in our previous work, despite their significantly lower IC_{50} values at *h*BChE.[11] BChE-inhibitor **1** was tested under the same conditions and showed only a tendency to an effect in the Y-maze test at 3 mg/kg and a significant effect in passive avoidance (p = 0.05) at 0.3 mg/kg.[11]

To further investigate possible off-target effects and to determine the in vivo selectivity for BChE inhibition in the **3c** mode of action, as well as of the multitarget approach, melatonin based hybrid **3c** was tested in homozygous BChE KO mice at a dosage of 0.3 mg/kg under the above conditions. As observed for the Swiss mice, icv injection of Aβ_{25-35} resulted in a memory deficit in the wildtype 129 Sv (WT) mouse strain in both the spontaneous alternation (Figure 7A)

https://doi.org/10.1021/acs.jmedchem.1c00534
J. Med. Chem. 2021, 64, 9302−9320

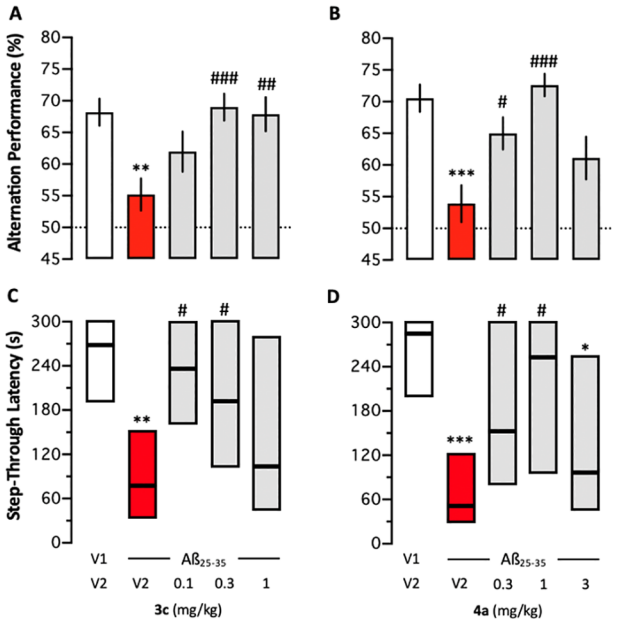

Figure 6. Effect of **3c** and **4a** on Aβ_{25-35} induced learning impairments in mice: spontaneous alternation performance (A, B) and passive avoidance response (C, D). Mice received Aβ_{25-35} (9 nmol, ICV) or vehicle 1 (3 μL of ddH_2O) on day 1 and then vehicle 2, compound **3c** (A, C) or **4a** (B, D) in the 0.1−3 mg/kg, IP dose range, o.d. between day 1 to 7. Mice were then tested for spontaneous alternation on day 8 and passive avoidance on day days 9 and 10. Data show mean ± SEM (A, B) or median and interquartile range (C, D). ANOVA: $F_{(4,61)} = 5.53$, $p < 0.001$, $n = 12-15$ per group in (A); $F_{(4,50)} = 8.16$, $p < 0.0001$, $n = 10-12$ in panel B. Kruskal−Wallis ANOVA: $H = 11.28$, $p < 0.05$, $n = 16-18$ in panel C; $H = 14.23$, $p < 0.01$, $n = 14-16$ in panel D. * $p < 0.05$, ** $p < 0.01$, *** $p < 0.001$ vs V1/V2-treated group; # $p < 0.05$, ## $p < 0.01$, ### $p < 0.001$ vs Aβ_{25-35}/V2-treated group; Dunnett's test in panels A and B; Dunn's test in panels C and D.

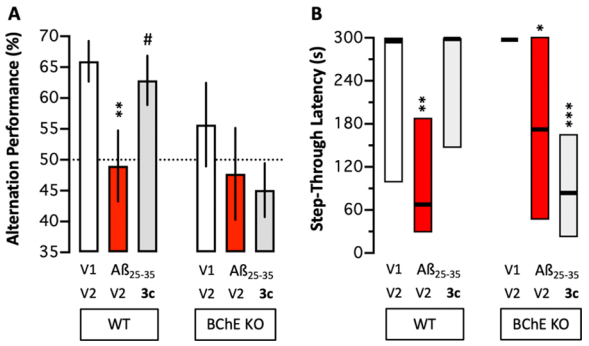

Figure 7. Effect of **3c** on Aβ_{25-35}-induced learning impairments in BChE KO mice: spontaneous alternation performance (A) and passive avoidance response (B). Mice received Aβ_{25-35} (9 nmol, ICV) or vehicle 1 (3 μL pf ddH_2O, V1) on day 1 and then vehicle 2 (H_2O/DMSO 1/1, V2) or the compound at 0.3 mg/kg, IP, o.d. between day 1 and 7. Mice were then tested for spontaneous alternation on day 8 and passive avoidance on day days 9 and 10. Data show mean ± SEM (A) or median and interquartile range (B). ANOVA: $F_{(2,27)} = 2.05$, $p < 0.05$ for WT, $F_{(2,26)} = 0.895$, $p > 0.05$ for BChE KO, $n = 7-13$ per group in (A). Kruskal−Wallis ANOVA: $H = 7.36$, $p < 0.05$ for WT, $H = 16.67$, $p < 0.001$ for BChE KO, $n = 6-15$ in (B). * $p < 0.05$, ** $p < 0.01$, *** $p < 0.001$ vs V1/V2-treated group; # $p < 0.05$ vs Aβ_{25-35}/V2-treated group; Dunnett's test in (A), Dunn's test in (B).

and passive avoidance responses (Figure 7B), which was prevented by administration of **3c**. In BChE KO mice, the ICV administration of Aβ_{25-35} aggregates caused a more moderate deficit in alternation (Figure 7A) and passive avoidance response (Figure 7B), but that was unaffected by **3e**, confirming the involvement of BChE inhibition in the effect of **3c**. These observations corresponds to our expectations, since (1) BChE KO mice were previously described by us to be less sensitive to Aβ_{25-35} toxicity[12] and (2) a reduced activity of **3c** was observed due to the lack of interaction with the main hybrid's target.

CONCLUSION

While the novel MTDLs showed a decreased IC_{50} value compared to the parent BChE inhibitor **1**, the half-life of the carbamylated BChE increased at the same time from 1.12 h up to 3 h for **3c**. The resulting MTDLs showed similar antioxidant properties compared to their parent antioxidant molecules in several physicochemical assays (DPPH, ORAC, and metal chelating). Regarding physicochemical antioxidant activities, different modes of action depending on the used antioxidative moiety were observed. Therefore, two representative hybrids (**3c** and **4a**) with different modes of antioxidant action were selected for further investigations. The hybrids showed no neurotoxic properties and protected the murine hippocampal HT22 cell line from induced intracellular oxidative stress, while the parent antioxidant moieties were inactive. Depending on the antioxidant moiety used, the protective effect was differently pronounced, with a significant effect at 5 μM for **3c**, and 10 μM for **4a**. Additionally, hybrids **3c** and **4a** lead to a reduction in LPS-induced microglia inflammation, showing an immunomodulatory effect with a parallel switch from neurotoxic M1 to neuroprotective M2 microglial phenotype, compared to the parent antioxidant moieties melatonin and ferulic acid. Both compounds were able to significantly protect mice of Aβ_{25-35} induced learning deficits at very low dosage regarding spatial working (**3c** and **4a** 0.3 mg/kg), as well as long-term memory (**3c** 0.1 mg/kg and **4a** 0.3 mg/kg). It should be noted at this point, that the hybrids show a significantly better in vivo efficacy compared to the BChE inhibitor **1**. The observed in vivo efficacy of the hybrids is comparable with the efficacy of previously described optimized BChE inhibitors, despite their higher IC_{50} values and a significant shorter half-life.[11] To further investigate the involvement of BChE inhibition as a key neuroprotectant, hybrid **3c** was tested at its effective dose (0.3 mg/kg) in BChE KO mice. As expected, no significant effect was observed, since part of the synergistic effect was removed through the BChE invalidation. The in vitro and in vivo studies confirm the successful application of the MTDL concept. Further development of the hybrids is encouraged by the fact that in addition to a pseudo-irreversible BChE inhibitor, melatonin itself is currently under clinical investigations for treating cognitive impairments and we herein were able to show that linkage of both result in a synergistic effect in vivo.[61−63]

EXPERIMENTAL SECTION

Chemistry. *General Information.* All reagents were used without further purification and purchased from common commercial suppliers. For anhydrous reaction conditions, CH_2Cl_2 was dried prior to use by refluxing over CaH_2 under argon atmosphere for at least 2 days. Thin-layer chromatography was carried out on silica gel 60 (aluminum oxide films with fluorescent indicator 254 nm). For

https://doi.org/10.1021/acs.jmedchem.1c00534
J. Med. Chem. 2021, 64, 9302−9320

detection, iodine vapor and UV light (254 and 366 nm) were used. For column chromatography, silica gel 60 (particle size 0.040−0.063 mm) was used. Nuclear magnetic resonance spectra were recorded with a Bruker AV-400 NMR instrument in $CDCl_3$ or MeOD and the chemical shifts are expressed in ppm relative to $CDCl_3$ (7.26 ppm for ^1H and 77.16 ppm for ^{13}C) or MeOD (3.31 ppm for ^1H and 49.0 ppm for ^{13}C). The purity was determined by HPLC (Shimadzu Products) containing a DGU-20A3R degassing unit, an LC20AB liquid chromatograph, and an SPD-20A UV/vis detector. The UV detection was measured at 254 nm. Mass spectra were obtained with a LCMS 2020 (Shimadzu Products). As the stationary phase, a Synergi 4U Fusion RP column 150 mm × 4.6 mm (Phenomenex) was used, and as the mobile phase, a gradient of MeOH (0.1% formic acid)/water (0.1% formic acid) was used. Parameters: A = water, B = MeOH, V (B)/(V (A) + V (B)) = from 5% to 90% over 10 min, V (B)/(V (A) + V (B) = 90% for 5 min, V (B)/(V (A) + V (B)) = from 90% to 5% over 3 min. The process was performed at a flow rate of 1.0 mL/min. Biologically characterized compounds had a purity of ≥95% and were screened for PAINS, indicating no assay interference.

*General Procedure I for the Boc-Protection and Amide Formation of Amino Acids (**7a−c**) to Melatonin Derivatives (**8a−c**).* The respective amino acid (1 equiv) was suspended in DMF; then, di-*tert*-butyl decarbonate and NEt_3 (1.1 equiv) were added. The mixture was treated with ultrasound at 40 °C until a clear solution was formed. This solution was then stirred for another 2 h at r.t. Then, the remaining NEt_3, 2-(5-methoxy-1*H*-indol-3-yl)ethan-1-amine, and HBTU were added. After stirring for 4 h at r.t., the solvent was removed in vacuo. The crude product was dissolved in CH_2Cl_2 and washed with 1 M $NaOH_{aq}$. Combined organic layers were dried over anhydrous $MgSO_4$, and the solvent was removed in vacuo.

*General Procedure II for the deprotection of Melatonin Derivatives (**8a−c**) to Amines (**9a−c**).* The respective protected amines **8a−c** were dissolved in 5% TFA in CH_2Cl_2 and stirred for 9 h at r.t. The solvent was removed in vacuo. The crude product was, then, washed with a 2 M $NaOH_{aq}$ solution, saturated with NaCl, and extracted with ethyl acetate. Combined organic layers were dried over anhydrous $MgSO_4$, and the solvent was removed in vacuo.

*General Procedure III for the Activation of Amines (**9a−c**) and (**12a,b**) to Activated Carbamates (**10a−c**) and (**13a,b**).* 4-Nitrophenyl chloroformate was dissolved in dry CH_2Cl_2 and cooled to 0 °C. After it was stirred for 10 min, NEt_3 (dried over $MgSO_4$ prior use) was added. This mixture was slowly added to a mixture of the respective amine in dry CH_2Cl_2 at 0 °C. After it was stirred for 10 min at 0 °C, the mixture was allowed to warm up to r.t. and stirred for further 2 h. After purification using column chromatography, the activated carbamate was directly used for further synthesis.

*General Procedure IV for Transfer of Activated Carbamates (**10a−c**) and (**13a,b**) to Carrier Scaffold (**2**) to Target Compounds (**3a−c**) and (**14a,b**).* 13-Methyl-5,8,13,13*a*-tetrahydro-6*H*-isoquinolino[1,2-*b*]quinazolin-10-ol **2** was synthesized as previously described[11,25,47] and dissolved in dry CH_2Cl_2. The mixture was cooled to 0 °C and NaH (60% dispersion in paraffin liquid). The mixture was stirred for 10 min and was then added to the respective activated carbamate, dissolved in dry CH_2Cl_2. The mixture stirred at r.t.; the solvent was removed in vacuo, and the crude product was purified using column chromatography.

*General Procedure V for Selective Mono Boc-Protection of Diamines (**11a,b**) to Protected Amines (**12a,b**).* The respective diamine was dissolved in CH_2Cl_2 (150 mL) and NEt_3 was added. Di-*tert*-butyl decarbonate was dissolved in ethyl acetate (50 mL) and, then, added to the reaction mixture using a syringe pump (14.2 mL/min). After complete addition, the mixture stirred for further 2 h at r.t. Then, the solvent was removed in vacuo, and the crude product dissolved in CH_2Cl_2 and washed with water. The combined organic layers were dried over anhydrous $MgSO_4$, and the solvent was removed in vacuo.

*General Procedure VI for Selective Boc-Cleavage of Carbamates (**14a,b**) and Amide Coupling with Respective Antioxidant Moieties to Target Compounds (**4a,b**), (**5a,b**), and (**6a,b**).* MeOH (8.58 mL) was cooled to 0 °C, and acetyl chloride (1.42 mL) was carefully added. The respective Boc-protected carbamate was dissolved in this solution and stirred at r.t. for 2.5 h. Then, the reaction mixture was transferred to a separation funnel and loaded with a mixture of sat. $NaHCO_3$/sat. NaCl aqueous solution (1:1) and CH_2Cl_2. The combined organic layers were dried over anhydrous $MgSO_4$, and the solvent was removed in vacuo. During the removal of CH_2Cl_2 in vacuo, the respective antioxidant moieties, HBTU and NEt_3, were suspended in another flask in CH_2Cl_2, and a clear solution was formed. The solution stirred for 15 min at r.t. and was then combined with the amine. The reaction mixture stirred at r.t. for 12 h. Then the solvent was removed in vacuo, and the crude product was purified using column chromatography.

*13-Methyl-5,8,13,13a-tetrahydro-6H-isoquinolino[1,2-b]-quinazolin-10-yl (3-((2-(5-Methoxy-1H-indol-3-yl)ethyl)amino)-3-oxopropyl)carbamate (**3a**).* The reaction was carried out according to general procedure IV, using 4-nitrophenyl (3-((2-(5-methoxy-1*H*-indol-3-yl)ethyl)amino)-3-oxopropyl)carbamate **10a** (67 mg, 0.16 mmol), 13-methyl-5,8,13,13a-tetrahydro-6*H*-isoquinolino[1,2-*b*]-quinazolin-10-ol **2** (35 mg 0.13 mmol), and NaH (5.6 mg, 0.14 mmol). The crude product was purified using column chromatography and CH_2Cl_2: MeOH: 25% NH_{3aq} (35: 1: 0.1) as mobile phase. The product 13-methyl-5,8,13,13*a*-tetrahydro-6*H*-isoquinolino[1,2-*b*]quinazolin-10-yl (3-((2-(5-methoxy-1*H*-indol-3-yl)ethyl)amino)-3-oxopropyl)carbamate **3a** (34 mg, 61 μmol, 47%) was obtained as a pale yellow oil.

^1H NMR (400 MHz, $CDCl_3$): δ = 8.13 (s, 1H), 7.39−7.34 (m, 1H), 7.26−7.20 (m, 3H), 7.17−7.13 (m, 1H), 7.03−6.98 (m, 2H), 6.90−6.84 (m, 3H), 6.72 (s, 1H), 5.79−5.71 (m, 2H), 4.89−4.82 (m, 1H), 4.01 (d, *J* = 15.3 Hz, 1H), 3.85 (s, 3H), 3.61 (dd, *J* = 12.6, 6.4 Hz, 2H), 3.52−3.47 (m, 1H), 3.33−3.23 (m, 1H), 3.17−3.01 (m, 1H), 2.95 (t, *J* = 6.7 Hz, 2H), 2.89−2.80 (m, 1H), 2.78−2.70 (m, 1H), 2.59 (s, 3H), 2.38 (t, *J* = 5.9 Hz, 2H), 1.33−1.26 (m, 2H) ppm.

^{13}C NMR (101 MHz, $CDCl_3$): δ = 171.3, 155.4, 154.3, 145.6, 144.3, 135.9, 133.8, 131.7, 129.0, 128.8, 127.81, 127.77, 126.0, 124.9, 123.0, 120.5, 119.9, 119.7, 112.61, 112.56, 112.2, 100.7, 76.4, 56.1, 47.9, 39.7, 38.0, 37.5, 35.9, 29.8, 25.4 ppm.

ESI: *m*/*z* calcd for $C_{32}H_{36}N_5O_4$ $[M + H]^+$, 554.28; found, 554.20; retention time 7.42 min, HPLC purity 96%.

*13-Methyl-5,8,13,13a-tetrahydro-6H-isoquinolino[1,2-b]-quinazolin-10-yl (5-((2-(5-Methoxy-1H-indol-3-yl)ethyl)amino)-5-oxopentyl)carbamate (**3b**).* The reaction was carried out according to general procedure IV, using 4-nitrophenyl (5-((2-(5-methoxy-1*H*-indol-3-yl)ethyl)amino)-5-oxopentyl)carbamate **10b** (171 mg, 0.36 mmol), 13-methyl-5,8,13,13*a*-tetrahydro-6*H*-isoquinolino[1,2-*b*]-quinazolin-10-ol **2** (48 mg 0.18 mmol), and NaH (14.3 mg, 0.36 mmol). The crude product was purified using column chromatography and CH_2Cl_2: MeOH: 25% NH_{3aq} (35: 1: 0.1) as mobile phase. The product 13-methyl-5,8,13,13*a*-tetrahydro-6*H*-isoquinolino[1,2-*b*]quinazolin-10-yl (5-((2-(5-methoxy-1*H*-indol-3-yl)ethyl)amino)-5-oxopentyl)carbamate **3b** (86 mg, 0.15 mmol, 82%) was obtained as a pale yellow oil.

^1H NMR (400 MHz, $CDCl_3$): δ = 8.58 (s, 1H), 7.37−7.33 (m, 1H), 7.25−7.20 (m, 2H), 7.20−7.12 (m, 2H), 7.01 (d, *J* = 2.1 Hz, 1H), 6.90 (d, *J* = 1.6 Hz, 1H), 6.90−6.85 (m, 2H), 6.86−6.81 (m, 1H), 6.74 (s, 1H), 5.86 (t, *J* = 5.2 Hz, 1H), 5.48 (t, *J* = 5.7 Hz, 1H), 4.77 (s, 1H), 3.95 (d, *J* = 15.4 Hz, 1H), 3.83 (s, 3H), 3.55 (dd, *J* = 12.4, 6.3 Hz, 2H), 3.27−3.13 (m, 3H), 3.11−3.01 (m, 1H), 2.89 (t, *J* = 6.6 Hz, 2H), 2.86−2.77 (m, 1H), 2.73−2.64 (m, 1H), 2.56 (s, 3H), 2.10 (t, *J* = 7.3 Hz, 2H), 1.67−1.56 (m, 2H), 1.53−1.43 (m, 2H), 1.34−1.18 (m, 1H) ppm.

^{13}C NMR (101 MHz, $CDCl_3$): δ = 173.0, 155.6, 154.0, 145.7, 144.3, 136.0, 133.9, 131.7, 128.9, 128.8, 127.8, 127.6, 125.9, 125.1, 123.2, 120.2, 119.8, 119.7, 112.4, 112.21, 112.16, 100.7, 76.3, 56.1, 47.7, 40.7, 39.7, 37.9, 36.0, 29.3, 28.5, 25.3, 22.8 ppm.

ESI: *m*/*z* calcd for $C_{34}H_{40}N_5O_4$ $[M + H]^+$, 582.31; found 582.25; retention time 7.72 min, HPLC purity 97%.

*13-Methyl-5,8,13,13a-tetrahydro-6H-isoquinolino[1,2-b]-quinazolin-10-yl (7-((2-(5-Methoxy-1H-indol-3-yl)ethyl)amino)-7-oxoheptyl)carbamate (**3c**).* The reaction was carried out according to general procedure IV, using 4-nitrophenyl (7-((2-(5-methoxy-1*H*-indol-3-yl)ethyl)amino)-7-oxoheptyl)carbamate **10c** (162 mg, 0.32

https://doi.org/10.1021/acs.jmedchem.1c00534
J. Med. Chem. 2021, 64, 9302−9320

mmol), 13-methyl-5,8,13,13a-tetrahydro-6*H*-isoquinolino[1,2-*b*]-quinazolin-10-ol **2** (43 mg 0.16 mmol), and NaH (10.3 mg, 0.26 mmol). The crude product was purified using column chromatography and CH_2Cl_2:MeOH: 25% $NH_{3\ aq}$ (35:1:0.1) as mobile phase. The product 13-methyl-5,8,13,13a-tetrahydro-6*H*-isoquinolino[1,2-*b*]quinazolin-10-yl (7-((2-(5-methoxy-1*H*-indol-3-yl)ethyl)amino)-7-oxoheptyl)carbamate **3c** (38 mg, 61 μmol, 38%) was obtained as a pale yellow oil.

^{1}H NMR (400 MHz, $CDCl_3$): δ = 8.60 (s, 1H), 7.38−7.35 (m, 1H), 7.25−7.20 (m, 2H), 7.20−7.13 (m, 2H), 7.01 (d, *J* = 2.2 Hz, 1H), 6.94 (d, *J* = 2.0 Hz, 1H), 6.92−6.86 (m, 2H), 6.84 (dd, *J* = 8.8, 2.3 Hz, 1H), 6.77 (d, *J* = 1.8 Hz, 1H), 5.71 (t, *J* = 5.1 Hz, 1H), 5.27 (t, *J* = 5.9 Hz, 1H), 4.80 (s, 1H), 3.99 (d, *J* = 15.6 Hz, 1H), 3.84 (s, 3H), 3.58 (dd, *J* = 12.5, 6.4 Hz, 2H), 3.27−3.15 (m, 3H), 3.13−3.02 (m, 1H), 2.92 (t, *J* = 6.6 Hz, 2H), 2.83 (dt, *J* = 16.3, 4.9 Hz, 1H), 2.73−2.66 (m, 1H), 2.57 (s, 3H), 2.09 (t, *J* = 7.4 Hz, 2H), 1.62−1.46 (m, 4H), 1.34−1.23 (m, 5H) ppm.

^{13}C NMR (101 MHz, $CDCl_3$): δ = 173.3, 155.6, 154.0, 145.8, 144.2, 136.0, 134.0, 131.8, 128.9, 128.8, 127.8, 127.6, 125.9, 125.7, 123.2, 120.4, 119.9, 119.7, 115.8, 112.33, 112.25, 100.6, 76.4, 56.1, 47.8, 41.2, 39.6, 37.9, 36.7, 29.7, 28.7, 28.6, 26.3, 25.6, 25.3 ppm.

ESI: *m*/*z* calcd for $C_{36}H_{44}N_5O_4$ $[M + H]^+$, 610.34; found 610.25; retention time 8.05 min, HPLC purity 97%.

*13-Methyl-5,8,13,13a-tetrahydro-6H-isoquinolino[1,2-b]-quinazolin-10-yl (E)-(4-(3-(4-Hydroxy-3-methoxyphenyl)-acrylamido)butyl)carbamate (**4a**).* The reaction was carried out according to general procedure VI, using *tert*-butyl (13-methyl-5,8,13,13*a*-tetrahydro-6*H*-isoquinolino[1,2-*b*]quinazolin-10-yl) butane-1,4-diyldicarbamate **14a** (100 mg, 0.21 mmol), HBTU (83 mg, 0.22 mmol), (*E*)-3-(4-hydroxy-3-methoxyphenyl)acrylic acid (42 mg, 0.22 mmol), and NEt_3 (31.8 μL, 0.23 mmol). The crude product was purified using column chromatography and CH_2Cl_2: MeOH: 25% NH_{3aq} (35: 1: 0.1) as mobile phase. The product 13-methyl-5,8,13,13*a*-tetrahydro-6*H*-isoquinolino[1,2-*b*]quinazolin-10-yl (*E*)-(4-(3-(4-hydroxy-3-methoxyphenyl)acrylamido)butyl)carbamate **4a** (107 mg, 0.19 mmol, 91%) was obtained as a pale yellow oil.

^{1}H NMR (400 MHz, $CDCl_3$): δ = 7.52 (d, *J* = 15.5 Hz, 1H), 7.38−7.33 (m, 1H), 7.25−7.18 (m, 2H), 7.15−7.11 (m, 1H), 6.99 (dd, *J* = 8.2, 1.6 Hz, 1H), 6.94 (d, *J* = 1.7 Hz, 1H), 6.91−6.83 (m, 3H), 6.76−6.72 (m, 1H), 6.27 (d, *J* = 15.6 Hz, 1H), 6.20−6.13 (m, 1H), 5.45 (t, *J* = 5.4 Hz, 1H), 4.80 (s, 1H), 3.97 (d, *J* = 15.3 Hz, 1H), 3.90−3.78 (m, 4H), 3.44−3.34 (m, *J* = 5.8 Hz, 2H), 3.31−3.18 (m, 3H), 3.11−3.01 (m, 1H), 2.85−2.76 (m, 1H), 2.75−2.64 (m, 1H), 2.55 (s, 3H), 1.68−1.54 (m, 4H), 1.34−1.20 (m, 1H) ppm.

^{13}C NMR (101 MHz, $CDCl_3$): δ = 166.7, 155.7, 147.6, 147.0, 145.8, 144.2, 141.0, 136.0, 134.0, 128.9, 128.8, 127.6, 127.4, 125.9, 125.2, 122.1, 120.4, 119.9, 119.7, 118.5, 115.0, 109.9, 76.4, 56.1, 56.0, 47.8, 40.9, 39.3, 37.9, 28.6, 27.4, 26.9 ppm.

ESI: *m*/*z* calcd for $C_{32}H_{37}N_4O_5$ $[M + H]^+$, 557.28; found 557.25; retention time 7.51 min, HPLC purity 95%.

*13-Methyl-5,8,13,13a-tetrahydro-6H-isoquinolino[1,2-b]-quinazolin-10-yl (E)-(6-(3-(4-Hydroxy-3-methoxyphenyl)-acrylamido)hexyl)carbamate (**4b**).* The reaction was carried out according to general procedure VI, using *tert*-butyl (13-methyl-5,8,13,13a-tetrahydro-6*H*-isoquinolino[1,2-*b*]quinazolin-10-yl) hexane-1,6-diyldicarbamate **14b** (100 mg, 0.20 mmol), HBTU (79 mg, 0.21 mmol), (*E*)-3-(4-hydroxy-3-methoxyphenyl)acrylic acid (40 mg, 0.21 mmol), and NEt_3 (31.6 μL, 0.23 mmol). The crude product was purified using column chromatography and CH_2Cl_2: MeOH: 25% NH_{3aq} (50: 1: 0.1) as mobile phase. The product 13-methyl-5,8,13,13*a*-tetrahydro-6*H*-isoquinolino[1,2-*b*]quinazolin-10-yl (*E*)-(6-(3-(4-hydroxy-3-methoxyphenyl)acrylamido)hexyl)carbamate **4b** (46 mg, 79 μmol, 40%) was obtained as a pale yellow oil.

^{1}H NMR (400 MHz, $CDCl_3$): δ = 7.51 (d, *J* = 15.5 Hz, 1H), 7.36−7.30 (m, 1H), 7.24−7.17 (m, 2H), 7.15−7.10 (m, 1H), 6.97 (d, *J* = 8.2 Hz, 1H), 6.93−6.81 (m, 4H), 6.77−6.71 (m, 1H), 6.27 (d, *J* = 15.6 Hz, 1H), 6.19 (t, *J* = 5.4 Hz, 1H), 5.37 (t, *J* = 5.7 Hz, 1H), 4.78−4.71 (m, 1H), 3.97 (d, *J* = 15.1 Hz, 1H), 3.87−3.78 (m, 4H), 3.35 (dd, *J* = 12.9, 6.5 Hz, 2H), 3.22 (dd, *J* = 12.8, 6.3 Hz, 3H), 3.10−2.99 (m, 1H), 2.84−2.75 (m, 1H), 2.74−2.61 (m, 1H), 2.52 (s, 3H), 1.59−1.47 (m, 4H), 1.39−1.32 (m, 4H), 1.27−1.22 (m, 1H) ppm.

^{13}C NMR (101 MHz, $CDCl_3$): δ = 166.6, 155.7, 147.6, 147.0, 145.7, 144.2, 140.7, 136.0, 133.9, 128.9, 128.8, 127.6, 127.5, 125.9, 125.1, 122.0, 120.4, 119.8, 119.7, 118.6, 115.0, 110.0, 76.3, 56.1, 55.9, 47.8, 40.8, 39.3, 37.8, 29.8, 29.5, 28.5, 26.1, 25.9 ppm.

ESI: *m*/*z* calcd for $C_{34}H_{41}N_4O_5$ $[M + H]^+$, 585.31; found 585.20; retention time 7.86 min, HPLC purity 95%.

*13-Methyl-5,8,13,13a-tetrahydro-6H-isoquinolino[1,2-b]-quinazolin-10-yl (4-Cinnamamidobutyl)carbamate (**5a**).* The reaction was carried out according to general procedure VI, using *tert*-butyl(13-methyl-5,8,13,13*a*-tetrahydro-6*H*-isoquinolino[1,2-*b*]-quinazolin-10-yl)butane-1,4-diyldicarbamate **14a** (100 mg, 0.21 mmol), HBTU (83 mg, 0.22 mmol), cinnamic acid (32 mg, 0.22 mmol), and NEt_3 (31.8 μL, 0.23 mmol). The crude product was purified using column chromatography and CH_2Cl_2: MeOH: 25% NH_{3aq} (40: 1: 0.1) as mobile phase. The product 13-methyl-5,8,13,13*a*-tetrahydro-6*H*-isoquinolino[1,2-*b*]quinazolin-10-yl (4-cinnamamidobutyl)carbamate **5a** (92 mg, 0.18 mmol, 87%) was obtained as a pale white oil.

^{1}H NMR (400 MHz, $CDCl_3$): δ = 7.54 (d, *J* = 15.6 Hz, 1H), 7.41−7.37 (m, 2H), 7.31−7.25 (m, 4H), 7.16−7.12 (m, 2H), 7.09−7.04 (m, 1H), 6.84−6.78 (m, 2H), 6.69 (d, *J* = 1.7 Hz, 1H), 6.33 (d, *J* = 15.6 Hz, 1H), 6.11−6.05 (m, 1H), 5.29 (t, *J* = 5.8 Hz, 1H), 4.74 (s, 1H), 3.92 (d, *J* = 15.5 Hz, 1H), 3.78 (d, *J* = 15.7 Hz, 1H), 3.34 (q, *J* = 6.2 Hz, 2H), 3.24−3.12 (m, 3H), 3.05−2.94 (m, 1H), 2.74 (dt, *J* = 16.2, 4.8 Hz, 1H), 2.67−2.59 (m, 1H), 2.48 (s, 3H), 1.98−1.65 (m, 1H), 1.63−1.45 (s, 5H) ppm.

^{13}C NMR (101 MHz, $CDCl_3$): δ = 166.3, 155.6, 145.9, 144.3, 141.0, 136.1, 135.0, 134.0, 132.4, 129.7, 128.9, 128.8, 127.9, 127.6, 125.9, 125.3, 121.0, 120.4, 120.0, 119.7, 76.5, 56.2, 47.9, 40.9, 39.4, 38.0, 28.7, 27.5, 26.9 ppm.

ESI: *m*/*z* calcd for $C_{31}H_{35}N_4O_3$ $[M + H]^+$, 511.27; found 511.35; retention time 7.84 min, HPLC purity 98%.

*13-Methyl-5,8,13,13a-tetrahydro-6H-isoquinolino[1,2-b]-quinazolin-10-yl (6-Cinnamamidohexyl)carbamate (**5b**).* The reaction was carried out according to general procedure VI, using *tert*-butyl(13-methyl-5,8,13,13a-tetrahydro-6*H*-isoquinolino[1,2-*b*]-quinazolin-10-yl)hexane-1,6-diyldicarbamate **14b** (84 mg, 0.17 mmol), HBTU (66 mg, 0.17 mmol), cinnamic acid (26 mg, 0.17 mmol), and NEt_3 (25.2 μL, 0.18 mmol). The crude product was purified using column chromatography and CH_2Cl_2: MeOH: 25% NH_{3aq} (50: 1: 0.1) as mobile phase. The product 13-methyl-5,8,13,13*a*-tetrahydro-6*H*-isoquinolino[1,2-*b*]quinazolin-10-yl (6-cinnamamidohexyl)carbamate **5b** (67 mg, 0.12 mmol, 75%) was obtained as a pale white oil.

^{1}H NMR (400 MHz, $CDCl_3$): δ = 7.63−7.56 (m, 1H), 7.47−7.41 (m, 2H), 7.35−7.29 (m, 4H), 7.24−7.17 (m, 2H), 7.15−7.11 (m, 1H), 6.94−6.83 (m, 2H), 6.75 (s, 1H), 6.43 (d, *J* = 13.0 Hz, 1H), 6.31 (t, *J* = 5.2 Hz, 1H), 5.38 (t, *J* = 5.8 Hz, 1H), 4.75 (s, 1H), 3.98 (d, *J* = 15.5 Hz, 1H), 3.84 (d, *J* = 15.7 Hz, 1H), 3.42−3.32 (m, 2H), 3.30−3.16 (m, 3H), 3.13−2.99 (m, 1H), 2.86−2.76 (m, 1H), 2.73−2.64 (m, 1H), 2.52 (s, 3H), 1.61−1.50 (m, 4H), 1.44−1.33 (m, 4H) ppm.

^{13}C NMR (101 MHz, $CDCl_3$): δ = 166.2, 155.7, 145.8, 144.3, 140.6, 136.0, 135.1, 133.9, 129.6, 128.9, 128.83, 128.80, 127.9, 127.5, 125.8, 125.2, 121.2, 120.4, 119.9, 119.6, 76.3, 56.2, 47.7, 40.8, 39.2, 37.8, 29.8, 29.5, 28.6, 26.1, 25.9 ppm.

ESI: *m*/*z* calcd for $C_{33}H_{39}N_4O_3$ $[M + H]^+$, 539.30; found 539.25; retention time 8.28 min, HPLC purity 96%.

*13-Methyl-5,8,13,13a-tetrahydro-6H-isoquinolino[1,2-b]-quinazolin-10-yl (4-(6-Hydroxy-2,5,7,8-tetramethylchromane-2-carboxamido)butyl)carbamate (**6a**).* The reaction was carried out according to general procedure VI, using *tert*-butyl (13-methyl-5,8,13,13*a*-tetrahydro-6*H*-isoquinolino[1,2-*b*]quinazolin-10-yl)-butane-1,4-diyldicarbamate **14a** (100 mg, 0.21 mmol), HBTU (83 mg, 0.21 mmol), 6-hydroxy-2,5,7,8-tetramethylchromane-2-carboxylic acid (55 mg, 0.22 mmol), and NEt_3 (31.8 μL, 0.23 mmol). The crude product was purified using column chromatography and CH_2Cl_2: MeOH: 25% NH_{3aq} (50: 1: 0.1) as mobile phase. The product 13-

https://doi.org/10.1021/acs.jmedchem.1c00534
J. Med. Chem. 2021, 64, 9302−9320

methyl-5,8,13,13*a*-tetrahydro-6*H*-isoquinolino[1,2-*b*]quinazolin-10-yl (4-(6-hydroxy-2,5,7,8-tetramethylchromane-2-carboxamido)butyl)-carbamate **6a** (87 mg, 0.14 mmol, 67%) was obtained as a yellow oil.

^{1}H NMR (400 MHz, $CDCl_3$): δ = 7.39−7.34 (m, 1H), 7.24−7.20 (m, 2H), 7.17−7.13 (m, 1H), 6.89 (s, 2H), 6.75 (s, 1H), 6.38 (t, *J* = 5.2 Hz, 1H), 5.07 (t, *J* = 5.7 Hz, 1H), 4.83 (s, 1H), 4.03 (d, *J* = 15.6 Hz, 1H), 3.88 (d, *J* = 15.7 Hz, 1H), 3.42−3.33 (m, 1H), 3.30−3.22 (m, 1H), 3.14−3.03 (m, 4H), 2.87−2.70 (m, 2H), 2.62−2.53 (m, 5H), 2.47−2.37 (m, 1H), 2.21−2.16 (m, 6H), 2.08 (s, 3H), 1.90−1.79 (m, 1H), 1.54 (s, 3H), 1.47−1.40 (m, 1H), 1.38−1.30 (m, 1H), 1.28−1.16 (m, 2H) ppm.

^{13}C NMR (101 MHz, $CDCl_3$): δ = 174.5, 155.4, 145.9, 145.8, 144.7, 144.3, 136.1, 134.0, 128.91, 128.85, 127.6, 125.9, 125.3, 124.6, 122.3, 121.9, 120.4, 119.9, 119.7, 118.4, 78.6, 76.3, 56.3, 47.9, 40.9, 38.6, 37.9, 29.8, 28.7, 27.1, 26.8, 25.0, 20.8, 12.5, 12.1, 11.5 ppm.

ESI: *m*/*z* calcd for $C_{36}H_{45}N_4O_5$ $[M + H]^+$, 613.34; found 613.25; retention time 8.19 min, HPLC purity 97%.

*13-Methyl-5,8,13,13a-tetrahydro-6H-isoquinolino[1,2-b]-quinazolin-10-yl (6-(6-Hydroxy-2,5,7,8-tetramethylchromane-2-carboxamido)hexyl)carbamate (**6b**).* The reaction was carried out according to general procedure VI, using *tert*-butyl(13-methyl-5,8,13,13*a*-tetrahydro-6*H*-isoquinolino[1,2-*b*]quinazolin-10-yl)-hexane-1,6-diyldicarbamate **14b** (118 mg, 0.23 mmol), HBTU (93 mg, 0.24 mmol), 6-hydroxy-2,5,7,8-tetramethylchromane-2-carboxylic acid (61 mg, 0.24 mmol), and NEt_3 (35.3 μL, 0.26 mmol). The crude product was purified using column chromatography and CH_2Cl_2: MeOH: 25% NH_{3aq} (60:1:0.1) as mobile phase. The product 13-methyl-5,8,13,13*a*-tetrahydro-6*H*-isoquinolino[1,2-*b*]quinazolin-10-yl (6-(6-hydroxy-2,5,7,8-tetramethylchromane-2-carboxamido)hexyl)-carbamate **6b** (44 mg, 70 μmol, 30%) was obtained as a yellow oil.

^{1}H NMR (400 MHz, $CDCl_3$): δ = 7.41−7.35 (m, 1H), 7.25−7.20 (m, 2H), 7.18−7.13 (m, 1H), 6.93−6.88 (m, 2H), 6.77 (s, 1H), 6.40−6.31 (m, 1H), 5.16 (t, *J* = 5.6 Hz, 1H), 4.85 (s, 1H), 4.04 (d, *J* = 15.5 Hz, 1H), 3.89 (d, *J* = 15.7 Hz, 1H), 3.42−3.32 (m, 1H), 3.31−3.23 (m, 1H), 3.17−2.99 (m, 4H), 2.84 (dt, *J* = 16.3, 4.8 Hz, 1H), 2.78−2.69 (m, 1H), 2.63−2.52 (m, 5H), 2.49−2.40 (m, 1H), 2.18 (d, *J* = 3.4 Hz, 6H), 2.08 (s, 3H), 1.85−1.77 (m, 1H), 1.54 (s, 3H), 1.42−1.32 (m, 4H), 1.20−1.12 (m, 2H), 1.02−0.93 (m, 2H) ppm.

^{13}C NMR (101 MHz, $CDCl_3$): δ = 174.4, 155.5, 145.9, 145.3, 144.5, 144.4, 136.1, 134.0, 128.91, 128.85, 127.6, 126.0, 125.3, 124.5, 122.1, 121.7, 120.4, 120.0, 119.7, 118.3, 78.6, 76.5, 56.3, 47.9, 41.3, 38.9, 38.0, 29.9, 29.8, 29.6, 28.7, 26.5, 26.1, 25.3, 20.9, 12.5, 12.1, 11.5 ppm.

ESI: *m*/*z* calcd for $C_{38}H_{49}N_4O_5$ $[M + H]^+$, 641.37; found 641.30; retention time 8.51 min, HPLC purity 95%.

*Tert-butyl(3-((2-(5-methoxy-1H-indol-3-yl)ethyl)amino)-3-oxopropyl)carbamate (**8a**).* The reaction was carried out according to general procedure I, using 3-aminopropanoic acid **7a** (100 mg, 1.12 mmol), di-*tert*-butyl decarbonate (244 mg, 1.12 mmol), NEt_3 (388 μL, 2.8 mmol), 2-(5-methoxy-1*H*-indol-3-yl)ethan-1-amine (313 mg, 1.12 mmol), and HBTU (466 mg, 1.23 mmol). The crude product was purified using column chromatography and CH_2Cl_2: MeOH: 25% NH_{3aq} (30: 1: 0.1) as mobile phase. The product *tert*-butyl(3-((2-(5-methoxy-1*H*-indol-3-yl)ethyl)amino)-3-oxopropyl)carbamate **8a** (405 mg, 1.12 mmol, quant.) was obtained as a pale brown oil.

^{1}H NMR (400 MHz, $CDCl_3$): δ = 8.39−8.25 (m, 1H), 7.24 (d, *J* = 8.8 Hz, 1H), 7.01 (d, *J* = 2.2 Hz, 1H), 6.99−6.95 (m, 1H), 6.85 (dd, *J* = 8.8, 2.2 Hz, 1H), 5.85 (s, 1H), 5.21 (s, 1H), 3.85 (s, 3H), 3.59−3.52 (m, 2H), 3.36 (dd, *J* = 12.0, 6.0 Hz, 2H), 2.91 (t, *J* = 6.9 Hz, 2H), 2.29 (t, *J* = 5.7 Hz, 2H), 1.42 (s, 9H) ppm.

^{13}C NMR (101 MHz, $CDCl_3$): δ = 171.5, 156.3, 154.1, 131.7, 127.8, 123.0, 112.51, 112.45, 112.2, 100.6, 79.5, 56.1, 39.7, 38.7, 36.4, 28.5, 25.4 ppm.

ESI: *m*/*z* calcd for $C_{19}H_{28}N_3O_4$ $[M + H]^+$, 362.21; found, 362.10; retention time 8.83 min.

*Tert-butyl(5-((2-(5-methoxy-1H-indol-3-yl)ethyl)amino)-5-oxopentyl)carbamate (**8b**).* The reaction was carried out according to general procedure I, using 5-aminopentanoic acid **7b** (500 mg, 4.27 mmol), di-*tert*-butyl decarbonate (932 mg, 4.27 mmol), NEt_3 (1.48 mL, 10.7 mmol), 2-(5-methoxy-1*H*-indol-3-yl)ethan-1-amine (812 mg, 4.27 mmol), and HBTU (1.78 g, 4.70 mmol). The crude product was purified using column chromatography and CH_2Cl_2: MeOH: 25% NH_{3aq} (30: 1: 0.1) as mobile phase. The product *tert*-butyl(5-((2-(5-methoxy-1*H*-indol-3-yl)ethyl)amino)-5-oxopentyl)carbamate **8b** (1.02 g, 2.61 mmol, 61%) was obtained as a pale brown oil.

^{1}H NMR (400 MHz, $CDCl_3$): δ = 9.03 (s, 1H), 7.20 (d, *J* = 8.8 Hz, 1H), 7.00 (d, *J* = 2.3 Hz, 1H), 6.92 (d, *J* = 2.0 Hz, 1H), 6.81 (dd, *J* = 8.8, 2.3 Hz, 1H), 6.04 (t, *J* = 5.2 Hz, 1H), 4.93−4.82 (m, 1H), 3.80 (s, 3H), 3.55−3.47 (m, 2H), 3.05−2.97 (m, 2H), 2.88 (t, *J* = 6.8 Hz, 2H), 2.05 (t, *J* = 7.4 Hz, 2H), 1.58−1.48 (m, 2H), 1.42 (s, 9H), 1.40−1.32 (m, 2H) ppm.

^{13}C NMR (101 MHz, $CDCl_3$): δ = 173.0, 156.3, 153.7, 131.7, 127.7, 123.1, 112.1, 112.0, 111.9, 100.5, 79.1, 55.9, 39.9, 39.7, 35.9, 29.4, 28.4, 25.2, 22.8 ppm.

ESI: *m*/*z* calcd for $C_{19}H_{28}N_3O_4$ $[M + H]^+$, 390.24; found, 390.15; retention time 9.08 min.

*Tert-butyl(7-((2-(5-methoxy-1H-indol-3-yl)ethyl)amino)-7-oxoheptyl)carbamate (**8c**).* The reaction was carried out according to general procedure I, using 7-aminoheptanoic acid **7c** (500 mg, 3.44 mmol), di-*tert*-butyl decarbonate (751 mg, 3.44 mmol), NEt_3 (1.19 mL, 8.6 mmol), 2-(5-methoxy-1*H*-indol-3-yl)ethan-1-amine (654 mg, 3.44 mmol), and HBTU (1.43 g, 3.78 mmol). The crude product was purified using column chromatography and CH_2Cl_2: MeOH: 25% NH_{3aq} (30: 1: 0.1) as mobile phase. The product *tert*-butyl (7-((2-(5-methoxy-1*H*-indol-3-yl)ethyl)amino)-7-oxoheptyl)carbamate **8c** (1.44 g, 3.44 mmol, quant.) was obtained as a pale brown oil.

^{1}H NMR (400 MHz, $CDCl_3$): δ = 9.46 (s, 1H), 7.16 (d, *J* = 8.8 Hz, 1H), 6.95 (d, *J* = 2.3 Hz, 1H), 6.89 (d, *J* = 2.0 Hz, 1H), 6.73 (dd, *J* = 8.8, 2.3 Hz, 1H), 6.31 (t, *J* = 5.6 Hz, 1H), 4.99 (s, 1H), 3.73 (s, 3H), 3.47 (dd, *J* = 12.8, 6.7 Hz, 2H), 2.99−2.91 (m, 2H), 2.84 (t, *J* = 6.9 Hz, 2H), 2.00 (t, *J* = 7.4 Hz, 2H), 1.51−1.42 (m, 2H), 1.37 (s, 9H), 1.34−1.24 (m, 2H), 1.17−1.09 (m, 4H) ppm.

^{13}C NMR (101 MHz, $CDCl_3$): δ = 173.2, 156.3, 153.9, 131.7, 127.7, 123.1, 112.3, 112.2, 112.0, 100.5, 79.0, 56.0, 39.8, 35.9, 29.5, 28.8, 28.4, 27.4, 26.2, 25.4, 22.6 ppm.

ESI: *m*/*z* calcd for $C_{23}H_{36}N_3O_4$ $[M + H]^+$, 418.27; found, 418.30; retention time 11.64 min.

*3-Amino-N-(2-(5-methoxy-1H-indol-3-yl)ethyl)propanamide (**9a**).* The reaction was carried out according to general procedure II, using *tert*-butyl (3-((2-(5-methoxy-1*H*-indol-3-yl)ethyl)amino)-3-oxopropyl)carbamate **8a** (405 mg, 1.12 mmol). The crude product was purified using column chromatography and CH_2Cl_2: MeOH: 25% NH_{3aq} (5: 1: 0.1) as mobile phase. The product 3-amino-*N*-(2-(5-methoxy-1*H*-indol-3-yl)ethyl)propanamide **9a** (293 mg, 1.12 mmol, quant.) was obtained as a pale brown oil.

^{1}H NMR (400 MHz, MeOD): δ = 10.08 (s, 1H), 7.94−7.83 (m, 1H) 7.24 (d, *J* = 8.8 Hz, 1H), 7.09 (d, *J* = 2.4 Hz, 1H), 7.03 (s, 1H), 6.78 (dd, *J* = 8.8, 2.4 Hz, 1H), 3.80 (s, 3H), 3.48 (t, *J* = 7.3 Hz, 2H), 2.91 (t, *J* = 7.3 Hz, 2H), 2.82 (t, *J* = 6.6 Hz, 2H), 2.27 (t, *J* = 6.6 Hz, 2H) ppm.

^{13}C NMR (101 MHz, MeOD): δ = 172.9, 153.6, 132.0, 127.8, 123.0, 111.8, 111.7, 111.2, 100.2, 55.1, 39.8, 38.1, 37.7, 24.2 ppm.

ESI: *m*/*z* calcd for $C_{14}H_{20}N_3O_2$ $[M + H]^+$, 262.16; found, 262.05; retention time 5.57 min.

*5-Amino-N-(2-(5-methoxy-1H-indol-3-yl)ethyl)pentanamide (**9b**).* The reaction was carried out according to general procedure II, using *tert*-butyl (5-((2-(5-methoxy-1*H*-indol-3-yl)ethyl)amino)-5-oxopentyl)carbamate **8b** (1.02 g, 2.61 mmol). The crude product was purified using column chromatography and CH_2Cl_2: MeOH: 25% NH_{3aq} (5: 1: 0.1) as mobile phase. The product 5-amino-*N*-(2-(5-methoxy-1*H*-indol-3-yl)ethyl)pentanamide **9b** (755 mg, 2.61 mmol, quant.) was obtained as a pale brown oil.

^{1}H NMR (400 MHz, MeOD): δ = 9.94 (s, 1H), 7.78 (t, *J* = 5.6 Hz, 1H), 7.13 (d, *J* = 8.8 Hz, 1H), 6.96 (d, *J* = 2.4 Hz, 1H), 6.92 (s, 1H), 6.65 (dd, *J* = 8.8, 2.4 Hz, 1H), 3.68 (s, 3H), 3.34 (t, *J* = 7.3 Hz, 2H), 2.82−2.71 (m, 4H), 2.09−2.02 (m, 2H), 1.51−1.45 (m, 4H) ppm.

^{13}C NMR (101 MHz, MeOD): δ = 175.2, 154.8, 133.2, 129.0, 124.3, 113.98, 112.95, 112.4, 101.5, 56.4, 41.2, 40.2, 36.0, 27.8, 26.1, 23.4 ppm.

https://doi.org/10.1021/acs.jmedchem.1c00534
J. Med. Chem. 2021, 64, 9302−9320

ESI: m/z calcd for $C_{16}H_{24}N_3O_2$ $[M + H]^+$, 290.19; found, 290.10; retention time 5.75 min.

*7-Amino-N-(2-(5-methoxy-1H-indol-3-yl)ethyl)heptanamide (**9c**).* The reaction was carried out according to general procedure II, using *tert*-butyl (7-((2-(5-methoxy-1*H*-indol-3-yl)ethyl)amino)-7-oxoheptyl)carbamate **8c** (1.43 g, 3.44 mmol). The crude product was purified using column chromatography and CH_2Cl_2: MeOH: 25% NH_{3aq} (5: 1: 0.1) as mobile phase. The product 7-amino-*N*-(2-(5-methoxy-1*H*-indol-3-yl)ethyl)heptanamide **9c** (1.09 g, 3.44 mmol, quant.) was obtained as a pale brown oil.

^{1}H NMR (400 MHz, MeOD): δ = 10.03 (s, 1H), 7.82 (t, J = 5.7 Hz, 1H), 7.21 (d, J = 8.8 Hz, 1H), 7.04 (d, J = 2.4 Hz, 1H), 6.99 (s, 1H), 6.72 (dd, J = 8.8, 2.4 Hz, 1H), 3.76 (s, 3H), 3.42 (t, J = 7.3 Hz, 2H), 2.86 (t, J = 7.3 Hz, 2H), 2.83−2.77 (m, 2H), 2.09 (t, J = 7.5 Hz, 2H), 1.57−1.46 (m, 4H), 1.28−1.17 (m, 4H) ppm.

^{13}C NMR (101 MHz, MeOD): δ = 176.0, 154.8, 133.3, 129.0, 124.3, 113.8, 112.99, 112.97, 112.4, 101.5, 56.4, 41.2, 40.6, 36.9, 29.4, 28.2, 26.9, 26.5, 26.1 ppm.

ESI: m/z calcd for $C_{18}H_{28}N_3O_2$ $[M + H]^+$, 318.22; found, 318.18; retention time 6.16 min.

*4-Nitrophenyl (3-((2-(5-Methoxy-1H-indol-3-yl)ethyl)amino)-3-oxopropyl)carbamate (**10a**).* The reaction was carried out according to general procedure III, using 3-amino-*N*-(2-(5-methoxy-1*H*-indol-3-yl)ethyl)propanamide **9a** (134 mg, 0.51 mmol), 4-nitrophenyl chloroformate (133 mg, 0.66 mmol), and NEt_3 (98 μL, 0.71 mmol). The crude product was purified using column chromatography and cyclohexane: ethyl acetate (2:1) as mobile phase. The product 4-nitrophenyl (3-((2-(5-methoxy-1*H*-indol-3-yl)ethyl)-amino)-3-oxopropyl)carbamate **10a** (67 mg, 0.16 mmol, 31%) was obtained as a pale yellow solid.

Spectral data and melting point not determined due to instability of the compound.

ESI: m/z calcd for $C_{21}H_{23}N_4O_6$ $[M + H]^+$, 427.16; found, 426.95; retention time 8.83 min.

*4-Nitrophenyl (5-((2-(5-Methoxy-1H-indol-3-yl)ethyl)amino)-5-oxopentyl)carbamate (**10b**).* The reaction was carried out according to general procedure III, using 5-amino-*N*-(2-(5-methoxy-1*H*-indol-3-yl)ethyl)pentanamide **9b** (492 mg, 1.70 mmol), 4-nitrophenyl chloroformate (377 mg, 1.87 mmol), and NEt_3 (471 μL, 34.0 mmol). The crude product was purified using column chromatography and cyclohexane: ethyl acetate (2: 1) as mobile phase. The product 4-nitrophenyl (5-((2-(5-methoxy-1*H*-indol-3-yl)ethyl)-amino)-5-oxopentyl)carbamate **10b** (171 mg, 0.36 mmol, 21%) was obtained as a pale yellow solid.

Spectral data and melting point were not determined because of the instability of the compound.

ESI: m/z calcd for $C_{23}H_{27}N_4O_6$ $[M + H]^+$, 455.19; found, 455.30; retention time 8.97 min.

*4-Nitrophenyl (7-((2-(5-Methoxy-1H-indol-3-yl)ethyl)amino)-7-oxoheptyl)carbamate (**10c**).* The reaction was carried out according to general procedure III, using 7-amino-*N*-(2-(5-methoxy-1*H*-indol-3-yl)ethyl)heptanamide **9c** (427 mg, 1.35 mmol), 4-nitrophenyl chloroformate (300 mg, 1.49 mmol), and NEt_3 (374 μL, 340 mmol). The crude product was purified using column chromatography and cyclohexane: ethyl acetate (2: 1) as mobile phase. The product 4-nitrophenyl (7-((2-(5-methoxy-1*H*-indol-3-yl)ethyl)-amino)-7-oxoheptyl)carbamate **10c** (162 mg, 0.32 mmol, 24%) was obtained as a pale yellow solid.

Spectral data and melting point were not determined because of the instability of the compound.

ESI: m/z calcd for $C_{25}H_{31}N_4O_6$ $[M + H]^+$, 483.22; found, 483.25; retention time 9.29 min.

*Tert-butyl(4-aminobutyl)carbamate (**12a**).* The reaction was carried out according to general procedure V, using butane-1,4-diamine **11a** (4.41 g, 50.0 mmol), di-*tert*-butyl decarbonate (2.18 g, 10.0 mmol), and NEt_3 (2.08 mL, 15.0 mmol). The crude product was purified using column chromatography and CH_2Cl_2: MeOH: 25% NH_{3aq} (7: 1: 0.1) as mobile phase. The product *tert*-butyl(4-aminobutyl)carbamate **12a** (892 mg, 4.74 mmol, 47%) was obtained as a colorless oil.

^{1}H NMR (400 MHz, $CDCl_3$): δ = 4.69 (s, 1H), 3.14−3.08 (m, 2H), 2.70 (t, J = 6.6 Hz, 2H), 1.52−1.47 (m, 4H), 1.42 (s, 9H) ppm.

^{13}C NMR (101 MHz, $CDCl_3$): δ = 156.2, 79.2, 41.9, 40.6, 30.9, 28.6, 27.6 ppm.

ESI: m/z calcd for $C_9H_{21}N_2O_2$ $[M + H]^+$, 189.16; not detected.

*Tert-butyl(6-aminohexyl)carbamate (**12b**).* The reaction was carried out according to general procedure V, using hexane-1,6-diamine **11b** (5.81 g, 50.0 mmol), di-*tert*-butyl decarbonate (2.18 g, 10.0 mmol), and NEt_3 (2.08 mL, 15.0 mmol). The crude product was purified using column chromatography and CH_2Cl_2: MeOH: 25% NH_{3aq} (7:1:0.1) as mobile phase. The product *tert*-butyl (6-aminohexyl)carbamate **12b** (2.03 g, 9.38 mmol, 94%) was obtained as a colorless oil.

^{1}H NMR (400 MHz, $CDCl_3$): δ = 4.56 (s, 1H), 3.13−3.03 (m, 2H), 2.66 (t, J = 6.9 Hz, 2H), 1.48−1.44 (m, 2H), 1.42 (s, 9H), 1.34−1.28 (m, 6H) ppm.

^{13}C NMR (101 MHz, $CDCl_3$): δ = 156.1, 79.1, 42.2, 40.6, 33.7, 30.2, 28.5, 26.7, 26.6 ppm.

ESI: m/z calcd for $C_{12}H_{25}N_2O_2$ $[M + H]^+$, 217.33; not detected.

*Tert-butyl(4-nitrophenyl)butane-1,4-diyldicarbamate (**13a**).* The reaction was carried out according to general procedure III, using *tert*-butyl(4-aminobutyl)carbamate **12a** (527 mg, 2.80 mmol), 4-nitrophenyl chloroformate (585 mg, 2.90 mmol), and NEt_3 (582 μL, 4.2 mmol). The crude product was purified using column chromatography and cyclohexane: ethyl acetate (2: 1) as mobile phase. The product *tert*-butyl(4-nitrophenyl)butane-1,4-diyldicarbamate **13a** (503 mg, 1.42 mmol, 51%) was obtained as a pale yellow solid.

Spectral data and melting point were not determined because of the instability of the compound.

ESI: m/z calcd for $C_{16}H_{23}N_3NaO_6$ $[M + Na]^+$, 354.17; found, 376.05; retention time 9.23 min.

*Tert-butyl(4-nitrophenyl)hexane-1,6-diyldicarbamate (**13b**).* The reaction was carried out according to general procedure III, using *tert*-butyl(6-aminohexyl)carbamate **12b** (755 mg, 3.49 mmol), 4-nitrophenyl chloroformate (738 mg, 3.66 mmol), and NEt_3 (726 μL, 5.24 mmol). The crude product was purified using column chromatography and cyclohexane: ethyl acetate (2: 1) as mobile phase. The product *tert*-butyl(4-nitrophenyl)hexane-1,6-diyldicarbamate **13b** (626 mg, 1.6 mmol, 47%) was obtained as a pale yellow solid.

Spectral data and melting point were not determined because of the instability of the compound.

ESI: m/z calcd for $C_{18}H_{27}N_3NaO_6$ $[M + Na]^+$, 404.18; found, 404.15; retention time 9.62 min.

*Tert-butyl(13-methyl-5,8,13,13a-tetrahydro-6H-isoquinolino-[1,2-b]quinazolin-10-yl)butane-1,4-diyldicarbamate (**14a**).* The reaction was carried out according to general procedure IV, using *tert*-butyl (4-nitrophenyl) butane-1,4-diyldicarbamate **13a** (503 mg, 1.42 mmol), 13-methyl-5,8,13,13*a*-tetrahydro-6*H*-isoquinolino[1,2-*b*]quinazolin-10-ol **2** (304 mg, 1.14 mmol), and NaH (57 mg, 1.42 mmol). The crude product was purified using column chromatography and CH_2Cl_2: MeOH: 25% NH_{3aq} (60: 1: 0.1) as mobile phase. The product *tert*-butyl(13-methyl-5,8,13,13*a*-tetrahydro-6*H*-isoquinolino[1,2-*b*]quinazolin-10-yl)butane-1,4-diyldicarbamate **14a** (443 mg, 0.90 mmol, 79%) was obtained as a colorless oil.

^{1}H NMR (400 MHz, $CDCl_3$): δ = 7.40−7.35 (m, 1H), 7.24−7.20 (m, 2H), 7.17−7.12 (m, 1H), 6.90 (s, 2H), 6.77 (s, 1H), 5.09 (s, 1H), 4.59 (s, 1H), 4.04 (d, J = 15.6 Hz, 1H), 3.89 (d, J = 15.7 Hz, 1H), 3.32−3.24 (m, 3H), 3.20−3.04 (m, 3H), 2.87−2.79 (m, 1H), 2.76−2.69 (m, 1H), 2.58 (s, 3H), 1.62−1.42 (m, 14H) ppm.

^{13}C NMR (101 MHz, $CDCl_3$): δ = 156.4, 156.2, 145.9, 144.3, 136.1, 128.94, 128.88, 127.6, 125.9, 125.3, 120.4, 120.0, 119.7, 76.5, 56.3, 47.9, 41.0, 38.0, 28.7, 28.6, 27.6 ppm.

ESI: m/z calcd for $C_{27}H_{37}N_4O_4$ $[M + H]^+$, 481.28; found, 481.30; retention time 7.76 min.

*Tert-butyl(13-methyl-5,8,13,13a-tetrahydro-6H-isoquinolino-[1,2-b]quinazolin-10-yl)hexane-1,6-diyldicarbamate (**14b**).* The reaction was carried out according to general procedure IV, using *tert*-butyl(4-nitrophenyl)hexane-1,6-diyldicarbamate **13b** (446 mg, 1.17 mmol), 13-methyl-5,8,13,13*a*-tetrahydro-6*H*-isoquinolino[1,2-*b*]quinazolin-10-ol **2** (249 mg, 0.94 mmol), and NaH (47 mg, 1.17

https://doi.org/10.1021/acs.jmedchem.1c00534
J. Med. Chem. 2021, 64, 9302−9320

mmol). The crude product was purified using column chromatography and CH_2Cl_2: MeOH: 25% NH_{3aq} (60:1:0.1) as mobile phase. The product *tert*-butyl(13-methyl-5,8,13,13*a*-tetrahydro-6*H*-isoquinolino[1,2-*b*]quinazolin-10-yl)hexane-1,6-diyldicarbamate **14b** (301 mg, 0.59 mmol, 45%) was obtained as a colorless oil.

^{1}H NMR (400 MHz, $CDCl_3$): δ = 7.44−7.38 (m, 1H), 7.29−7.23 (m, 2H), 7.21−7.16 (m, 1H), 6.95 (s, 2H), 6.81 (d, J = 1.1 Hz, 1H), 5.62 (t, J = 5.3 Hz, 1H), 4.87−4.85 (m, 1H), 4.05 (d, J = 15.5 Hz, 1H), 3.91 (d, J = 15.7 Hz, 1H), 3.34−3.22 (m, 3H), 3.18−3.06 (m, 3H), 2.93−2.83 (m, 1H), 2.80−2.73 (m, 1H), 2.62 (s, 3H), 1.59−1.46 (m, 14H), 1.40−1.30 (m, 4H) ppm.

^{13}C NMR (101 MHz, $CDCl_3$): δ = 156.2, 155.4, 145.5, 144.2, 135.8, 133.8, 128.8, 128.6, 127.5, 125.8, 124.9, 120.3, 119.6, 115.6, 76.2, 55.9, 47.6, 41.0, 40.3, 37.7, 29.9, 29.6, 28.4, 28.3, 26.2 ppm.

ESI: m/z calcd for $C_{29}H_{41}N_4O_4$ $[M + H]^+$, 509.31; found, 509.25; retention time 8.16 min.

DPPH Assay. Compound stock solutions were prepared in DMSO (5 mM) and diluted in MeOH. To 100 μL of the compound dilution, 33.3 μL of DPPH [200 μM] (Sigma-Aldrich, Munich, Germany) were added and incubated for 30 min at r.t. Ascorbic acid served as reference.[64] After incubation, the absorbance at 517 nm was determined with a multiwell plate photometer (Tecan, SpectraMax 250).

Statistical Analysis. Data are expressed as means ± SD of three independent experiments, each DPPH scavenging (%) against logarithmic compound concentration.

ORAC Assay. ORAC-capacity was investigated according to literature procedure with minor changes.[65,66] The assay was performed in 75 mM PBS (pH 7.4); the final volume was 200 μL, and incubation was at 37 °C. Fluorescein (FL) was used as a fluorescent probe; Trolox was used as the reference, and compound 2,2′-azobis(amidinopropane) dihydrochloride (AAPH) was used as the free radical generator. Compound dilution (20 μL) and FL (120 μL, 70 nM, final concentration) were combined in a black 96-well-microplate and preincubated for 15 min at 37 °C. Subsequently, AAPH solution (60 μL, 12 mM, final concentration) was added rapidly, and the plate was placed in a TECAN microplate reader to measure fluorescence (485 nm excitation and 510 nm emission filters) intensity every two min for 90 min. Samples were measured at two different concentrations (2 and 4 μM). A blank (FL + AAPH in PBS), and a calibration curve of Trolox (1, 2, 4, 6, 8, 10, 12, and 15 μM) was included in each experiment. All samples were prepared in duplicate and three independent assays were performed for each compound. The area under the fluorescence decay curve (fluorescence vs time) (AUC) was calculated as

$$\mathrm{AUC} = 1 + \sum_{i=1}^{i=45} f_i/f_0$$

where f_0 is the initial fluorescence reading at 0 min and f_i is the fluorescence reading at time 2i. The net AUC corresponding to a sample was calculated by subtracting the AUC corresponding to the blank (net AUC = $\mathrm{AUC_{antioxidant}} - \mathrm{AUC_{blank}}$). Linear regression equations were calculated by plotting the net AUC against the Trolox antioxidant standard concentration. ORAC-FL values were expressed as Trolox equivalents by using the standard curve calculated for each assay, where the ORAC-FL value of Trolox was taken as 1, plot the Trolox standard curve and interpolate it to determine sample ORAC values.

Inhibition of *h*BChE and *h*AChE. ChE inhibition was investigated using a modified Ellman's assay.[24,48,49] BChE (E.C. 3.1.1.8, from humans) was kindly provided by Oksana Lockridge from the University of Nebraska Medical Center. *h*AChE (EC 3.1.1.7, recombinant expressed) was purchased from Sigma-Aldrich. DTNB (Ellman's reagent); ATC and BTC iodides were obtained from Fluka Analytical. The readout was performed on a multiwell plate photometer (Tecan SpectraMax 250). Buffer I was freshly prepared before use (55 mM NaH_2PO_4, 0.3 mM DTNB, in ddH_2O, pH = 8.0 adjusted with 0.5 M $NaOH_{aq}$). Buffer II (55 mM NaH_2PO_4, in ddH_2O, pH = 8.0 adjusted with 0.5 M $NaOH_{aq}$).

IC_{50}-Determination. Enzymes were diluted in PBS containing 1 mg/mL bovine serum albumin (Sigma-Aldrich) for stabilization, to give stock solutions with 2.5 U/mL, which were stored at 7 °C until usage. Compound dilutions were prepared in a clear 96-well plate using buffer I. To 120 μL of the compound dilution, 10 μL of enzyme (2.5 U/min) was added in each well using a multidispenser. After 20 min of incubation at r.t., 3 μL of the respective substrate (ATC or BTC) [75 mM] were rapidly added in each well using a multidispenser. After substrate addition, the plate was directly shaken for 10 s before the first read and a kinetic measurement (read each 30 s for 3 min at 412 nm) was performed. Replacing the 120 μL of compound dilution with 120 μL of buffer I served as 100% enzyme activity. The enzyme activity of each concentration was calculated using the slope. IC_{50} values were calculated using GraphPad Prism 5 software by plotting enzyme activity against logarithmic inhibitor concentration. Values are presented as means ± SEM of at least three independent determinations.

Decarbamylation. To investigate the decarbamylation, 4 μL of a high concentrated enzyme solution (after 1000-fold dilution 2.5 U/min) were combined with 3 μL of a compound dilution in DMSO, which fully carbamylates the enzyme, in 193 μL of buffer II. The mixture incubated for 1 h at r.t. and was then diluted 1000-fold in buffer I, so that only decarbamylation and no further carbamylation is taking place from this time point on. The dilution was rapidly aliquoted in 8 wells (200 μL in each well) of a clear 96-well plate using a multidispenser. At the respective time points, 3 μL of the substrate (ATC or BTC) [75 mM] were rapidly added using a multidispenser, and the plate was directly shaken for 10 s before the first read, and a kinetic measurement (read each 30 s. for 3 min at 412 nm) was performed. First measurement was performed 5 min after the 1000-fold dilution and enzyme activity was always below 85%. When the enzyme activity was above 85%, the compound concentration was increased in the carbamylation step. Treatment of the enzyme with only 3 μL in DMSO instead of the compound served as 100% enzyme activity. Since the enzyme activity decreases over the time, the 100% activity control was also measured at each time point. The enzyme activity in percent was plotted against the time after 1000-fold dilution to obtain a function of first order. The half-life of carbamylated enzyme was calculated using GraphPad Prism 5.0 software. All procedures used to determine the inhibitory properties have been established before.[11,24,46] Values are presented as means ± SEM of at least three independent determinations.

Metal Chelating Assay. The chelating ability of Fe^{2+} was determined as described by Santos et al. with minor modifications.[67] Fe^{2+} of ferrous sulfate reacts with ferrozoine (3-(2-pyridyl)-5,6-diphenyl-1,2,4-triazine-*p*,*p*′-disulfonic acid monosodium salt hydrate) to form a purple Fe^{2+}-ferrozoine complex with absorption maximum at 562 nm. Presence of chelators reduces the formation of Fe^{2+}-ferrozoine complex. Lower absorbance at 562 nm indicates higher metal-chelating activity. To start the reaction, $FeSO_4$ solution (50 μL, 80 μM in 50 mM NaAc aqueous buffer pH 6.0) was added to diluted compounds (100 μL, in MeOH) or pure methanol as negative control. The 96-well plate was incubated at r.t. for 2 min, and ferrozine (50 μL, 250 μM in 50 mM NaAc aqueous buffer pH 6.0) was added to each well. After incubation for 10 min, the absorbance was measured with a microplate reader at 562 nm. The mixture of a dilution series of the compound and Fe^{2+} aq. served as a blank of the particular compound. EDTA·2Na in water was diluted with MeOH, which served as reference under the same assay conditions. Data is presented as mean ± SEM of two independent experiments, each performed in duplicate.

The ability of compounds to chelate Cu^{2+} was assessed using the method described by Santos et al. with minor modifications.[67] Free Cu^{2+} reacts with pyrocatechol violet (PV) at a proportion of 2:1, forming a blue-colored complex with an absorption maximum at 632 nm. Briefly, in each well, $CuSO_4$ (50 μL, 400 μM, in 50 mM NaAc aqueous buffer pH 6.0) was added to diluted compounds (100 μL in MeOH) or pure methanol as negative control. The 96-well-plate was incubated at r.t. for 2 min; then, PV (50 μL, 400 μM in 50 mM NaAc aqueous buffer pH 6.0) was added to each well. After incubation at r.t.

https://doi.org/10.1021/acs.jmedchem.1c00534
J. Med. Chem. 2021, 64, 9302−9320

for 10 min in the dark, absorbance was measured with a microplate reader at 632 nm. The experiments were performed in duplicates. EDTA·2 Na in water was diluted with MeOH, which was served as reference under the same assay conditions. Data is presented as mean ± SEM of two independent experiments, each performed in duplicate.

Neurotoxicity and Neuroprotection on HT22 Cells. *Cell Culture.* HT22 cells were grown in Dulbecco's modified Eagle's medium (DMEM, Sigma-Aldrich, Munich, Germany) supplemented with 10% (V/V) heat-inactivated fetal calf serum (FCS) and 1% (V/V) penicillin/streptomycin. Cells were passaged every 2 days (1:10) and incubated at 37 °C with 5% CO_2 in a humified incubator. Compounds were dissolved in pure DMSO and then diluted with medium. Generally, 80% confluent cells were detached using trypsine/EDTA and seeded with 5000 cells/well into a sterile, clear 96-well plate. After incubation in humidor for 24 h, cells were used for experiments.

Neurotoxicity. The growth medium was discarded, and different concentrations of the compound, diluted in growth medium, were added to the wells. DMSO (0.5%) in DMEM served as control. Cells were incubated for 24 h with the compound dilutions, then an MTT assay was performed.

Neuroprotection. The growth medium was discarded, and different concentrations of the compound, diluted in growth medium containing 5 mM glutamate (monosodium-L-glutamate, Sigma-Aldrich, Munich, Germany). DMSO (0.5%) in growth medium served as control. Glutamate 5 mM in growth medium served as negative control. Quercetin (25 μM, Sigma-Aldrich, Munich, Germany) served as positive control for neuroprotection. After incubation in humidor for 24 h, cells were used for experiments.

MTT Assay. Cell viability was investigated using MTT assay. Therefore, a 4 mg/mL stock of MTT in PBS was freshly prepared and diluted 1:10 with growth medium. After the cells were treated for 24 h, the dilutions were discarded and MTT in growth medium was added. Cells were incubated for 3 h, and then, the MTT solution was carefully discarded and replaced with an aqueous 10% SDS solution. After incubation for 12 h, absorbance at 560 nm of lysed cells was determined with a multiwell plate photometer (Tecan, SpectraMax 250).

Statistical Analysis. Results are presented as percentage of 0.5% DMSO treated control cells. Data are expressed as means ± SD of three independent experiments, each performed in sextuplicate. Analysis was accomplished using GraphPad Prism 5 software applying one-way ANOVA, followed by Dunnett's multiple comparison post-test. Levels of significance: *$p < 0.05$; ** $p < 0.01$; ***$p < 0.001$.

Immunomodulation Analysis on Microglia Cells. *Immunomodulation.* To evaluate the immunomodulatory effects of antioxidant parent moieties, melatonin and ferulic acid, and the resulting hybrids **3c** and **4a**, 2.5×10^5 mouse N9-microglial cells were plated in 35 mm dish in complete Dulbecco Modified Eagle Medium (DMEM supplemented with 10% heat inactivated Fetal Bovine Serum (FBS), 1% penicillin/streptomycin, 2 mM glutamine; all from Aurogene Srl, Rome, Italy), in the presence of 100 ng/mL LPS (lipopolysaccharide) and increasing concentrations of compounds. After 24 h, conditioned medium was collected to perform nitrite measurement, or concentrated through Microcon YM-3 (Millipore, Billerica, MA) and resuspended in 4× loading buffer (0.2 M Tris-HCL pH 6.8; sodium dodecyl sulfate; 40% glycerol; 0.4% bromophenol blue and 0.4 M dithiothreitol; Sigma-Aldrich) for Western Blot analysis. Similarly, microglial cells were collected in lysis buffer (1% SDS; 50 mM Tris pH 7.4; 1 mM EDTA; 1× protease and phosphatase inhibitor cocktails, Sigma-Aldrich), and the protein's amount was determined by using the Lowry protein assay.

For Western blot analysis, both media and cells samples were briefly sonicated with a Branson 250 digital sonifier, loaded into 12% sodium-dodecyl sulfate-polyacrylamide gels (SDS-PAGE; Bio-Rad), and transferred onto nitrocellulose membranes (GE Healthcare, Milano, Italy). After blocking nonspecific sites for 1 h in PBS−0.1% Tween-20 (Sigma-Aldrich) and 4% nonfat dry milk (Bio-Rad) at room temperature, the membranes were incubated with primary antibodies overnight at 4 °C in PBS−0.1% Tween-20: rabbit anti-iNOS (1:1000, Cell Signaling Technology, Danvers, Massachusetts, USA), mouse anti-TGFβ2 (1:1000 Abcam, Cambridge, UK), rabbit anti-TREM2 (1:1000, Cell Signaling Technology), and mouse anti-GAPDH (1:20000, Dako North America, Agilent Technologies, USA). The day after, specific horseradish peroxidase-conjugated antibodies (goat antirabbit and goat-anti mouse, 1:5000, Jackson ImmunoResearch, Cambridge, UK) were added 90 min at RT in PBS−0.1% Tween-20. Proteins were visualized through the Clarity Western ECL Substrate (Bio-Rad) and detected by using Bio-Rad Image Lab Software with a ChemiDoc imaging system (Bio-Rad).

Nitrite Measurement. NO accumulation in microglial conditioned media was indirectly quantified in 96-well-plates through a colorimetric assay based on Griess diazotization reaction. Known concentrations of $NaNO_2$ were used as standard curve. To quantify nitrites release formed by spontaneous oxidation of NO, 5 mM sulfanilamide (Sigma-Aldrich) was added to both culture media and $NaNO_2$; in the presence of nitrites, it generates a diazonium cation that subsequently couples to *N*-1-naphthylethylenediamine dihydrochloride 40 mM (NEDA; Sigma-Aldrich) producing a colored azo dye. Plates were then incubated 15 min at RT away from lights and absorbance was read at 540 nm with a Multiplate Spectrophotometric Reader (Biorad Laboratories Srl, Milano, Italy).

Statistical Analysis. All quantitative data are means ± SE from 3 independent experiments. Statistical analysis between treatments were calculated with GRAPHPAD PRISM6 (L Jolla, California, USA) by using one-way analysis of variance (ANOVA), followed by post hoc comparison Bonferroni's test. $p < 0.05$ value was considered statistically significant.

Statistical Analysis. All quantitative data are means ± SE from 3 independent experiments. Statistical analysis between treatments were calculated with GRAPHPAD PRISM6 (L Jolla, California, USA) by using one-way analysis of variance (ANOVA), followed by posthoc comparison Bonferroni's test. $p < 0.05$ value was considered statistically significant.

In Vivo Studies. To investigate possible in vivo neuroprotection against ICV injection of oligomerized Aβ_{25-35} peptide of **3c** and **4a** in vivo, each compound was injected IP o.d. between day 1 and 7. The peptide was ICV injected on day 1, and behavioral examination was performed between days 8 and 10. All animals were sacrificed on day 11 (cf., Figure S2)

Animals. Male Swiss mice, 6 weeks old and weighing 34−39 g, from Javier (Saint-Berthvin, France), were kept or housed and experiments took place within the animal facility building of the University of Montpellier (CECEMA, Office of Veterinary Service agreement #B-34-172-23). Homozygous BuChE KO founders were generously provided by Dr O. Lockridge (Eppley Institute, University of Nebraska Medical Center, Omaha, NE, USA).[68] The colony was then maintained on a pure 129 Sv strain at the animal facility of INRA in Montpellier (agreement no. D34-172-10). Litter mates were transferred to the animal facility of the University of Montpellier at the age of 3 months, at least 1 week before the behavioral experiments start. Animals were housed in groups with access to food and water ad libitum, except during behavioral experiments. They were kept in a temperature and humidity-controlled animal facility on 12 h/12 h light/dark cycle (lights off at 07:00 pm). All animal procedures were conducted in strict adherence to the European Union directive of September 22, 2010 (2010/63/UE) and authorized (file no. 1485-15034) by the National Ethic Committee (Paris, France).

Amyloid Peptide Preparation and Injection. Homogeneous oligomeric preparation of Aβ_{25-35} peptide was performed by incubation for 4 days at 37 °C according to Maurice et al.[59] For ICV injection, the mice were anesthetized with isoflurane 2.5%. Then Aβ_{25-35} (3 μL/mouse, 9 nmol/mouse) or vehicle solution (V1, ddH_2O 3 μL/mouse) was injected according to the previously described method.[59,69−73] It is well established that a vehicle solution similar as to a control scrambled Aβ_{25-35} peptide failed to induce toxicity and, therefore, affect learning abilities; vehicle-treated animals served as controls.[29,59,69−73]

Compound Preparation. Stock solutions of compounds were prepared in pure DMSO (4 mg/mL) and stored for 1 week at 4 °C.

https://doi.org/10.1021/acs.jmedchem.1c00534
J. Med. Chem. 2021, 64, 9302−9320

The injection dilutions were made fresh daily by diluting the stock solution with ddH_2O/DMSO. The final percentage of DMSO of 3 mg/kg dose was 50%. Vehicle solution used for control groups (V2) was DMSO 50% in ddH_2O.

Spontaneous Alternation Performance. On day 8, all animals were tested for spontaneous alternation performance in the Y maze, an index of spatial working memory. The Y maze used is made of gray poly(vinyl chloride). Each arm is 40 cm long, 13 cm high, 3 cm wide at the bottom, 10 cm wide at the top, and converging at an equal angle. Each mouse was placed at the end of one arm and allowed to move freely through the Y maze during an 8 min session. The series of arm entries, including possible returns into the same arm, was observed visually. Alternation was defined as entries into all thee arms on consecutive occasion. The number of maximum alternation is, therefore, the total number of arm entries minus two, and the percentage of alternation was calculated as (actual alternation/maximum alternations) × 100. Parameters included the percentage of alternation (memory index) and the total number of arm entries (exploration index).[50,59,60,62,63] Animals that shown an extreme behavior (alternation performance od <20% or >90% or number of arm entries <10) were discarded from the calculation. In this study, 5animals were discarded accordingly (2.7% attrition).

Passive Avoidance Test. On day 9 and 10, a passive avoidance test was performed. The apparatus is a two-compartment (each compartment 15 × 20 × 15 cm high) box with one white poly(vinyl chloride) walls and a black painted compartment. The black compartment contains a grid on the bottom, coupled to a shock generator scrambler (Lafayette Instruments, Lafayette, USA). The white compartment is lighted with a 60 W lamp positioned 40 cm above the apparatus during the experiment, while the black compartment is covered and dark. Compartments are separated by a guillotine door. On day 9, mice were trained by placing them in the lighted white compartment with initially closed guillotine door. After 5 s, the door was raised. When the mouse entered the black, dark compartment and placed all its paws on the grid floor, the door was closed, and the foot shock was delivered (0.3 mA for 3 s). The mouse was then directly placed back into its housing. The step-through latency, that is, the latency spent to enter the darkened compartment, and the number of vocalizations was recorded. The retention test was performed 24 h after training session on day 10. Each mouse was placed again into the lighted white compartment. After 5 s, the door was raised. The step-through latency was recorded up to 300 s. Animals that show latencies during the training and retention sessions lower than 10 s are considered as ailing to respond to the procedure and were discarded from the calculations. In this study, 2 animals were discarded accordingly (1% attrition).

■ ASSOCIATED CONTENT

Supporting Information

The Supporting Information is available free of charge at https://pubs.acs.org/doi/10.1021/acs.jmedchem.1c00534.

HPLC traces of all target compounds (PDF)

Molecular formula strings (CSV)

■ AUTHOR INFORMATION

Corresponding Author

Michael Decker − *Pharmaceutical and Medicinal Chemistry, Institute of Pharmacy and Food Chemistry, Julius Maximilian University of Würzburg, Am Hubland 97074, Würzburg, Germany;* orcid.org/0000-0002-6773-6245; Phone: +49-931-31-89676; Email: michael.decker@uni-wuerzburg.de

Authors

Matthias Scheiner − *Pharmaceutical and Medicinal Chemistry, Institute of Pharmacy and Food Chemistry, Julius Maximilian University of Würzburg, Am Hubland 97074, Würzburg, Germany*

Matthias Hoffmann − *Pharmaceutical and Medicinal Chemistry, Institute of Pharmacy and Food Chemistry, Julius Maximilian University of Würzburg, Am Hubland 97074, Würzburg, Germany*

Feng He − *Pharmaceutical and Medicinal Chemistry, Institute of Pharmacy and Food Chemistry, Julius Maximilian University of Würzburg, Am Hubland 97074, Würzburg, Germany*

Eleonora Poeta − *Department of Pharmacy and Biotechnology, University of Bologna, 40126 Bologna, Italy*

Arnaud Chatonnet − *DMEM, University of Montpellier, INRAE, 34060 Montpellier, France*

Barbara Monti − *Department of Pharmacy and Biotechnology, University of Bologna, 40126 Bologna, Italy;* orcid.org/0000-0003-0330-482X

Tangui Maurice − *MMDN, University of Montpellier, INSERM, EPHE, 34095 Montpellier, France*

Complete contact information is available at: https://pubs.acs.org/10.1021/acs.jmedchem.1c00534

Author Contributions

Design, synthesis of the target compounds, DPPH-assay, neurotoxicity and neuroprotection on HT22, and inhibitory potency on BChE and AChE were performed by M.S. In vivo experiments were performed by M.S., M.H., and T.M. BChE KO mice were generated by A.C. ORAC- and metal chelating assays were performed by F.H. Microglia effects were investigated by E.P. and B.M.; M.D. was responsible for the concept and organization of the project. All authors contributed to writing the manuscript, read and approved the final version.

Funding

M.D. acknowledges the German Research Council (Deutsche Forschungsgemeinschaft) under DFG DE 1546/6-3. M.D. and T.M. acknowledge support from Campus France (PHC Procope) and the German Academic Exchange Service (DAAD) with funds of the Federal Ministry of Education and Research (BmBF) under 57387204, as well as from BayFrance (Franco-Bavarian University cooperation center) under FK03-2020. A Ph.D. scholarship from the German Academic National Foundation (Studienstiftung des deutschen Volkes) was awarded to M.H., and support by the International Doctoral Program "Receptor Dynamics" of the Elite Network of Bavaria (Elitenetzwerk Bayern) is acknowledged by M.D. and M.H. M.S. acknowledges the French Embassy for funding his stay in Montpellier with the Procope Mobility Program.

Notes

The authors declare no competing financial interest.

■ ACKNOWLEDGMENTS

We thank O. Lockridge (University of Nebraska Medical Center) for providing human BChE and BChE KO breeders. We thank the animal facilities of the University of Montpellier, CECEMA, and DMEM for the animal housing and experimentation facility.

■ ABBREVIATIONS USED

AD, Alzheimer's disease; ACh, acetylcholine; AChE, acetylcholinesterase; ANOVA, analysis of variance; Aβ, amyloid

beta; ATC, acetylthiocholine; BChE, butyrylcholinesterase; Boc_2O, di-*tert*-butyl decarbonate; BTC, butyrylthiocholine; ChE, cholinesterase; CNS, central nervous system; DMEM, Dulbecco's modified Eagle's medium; DMF, *N*,*N*-dimethylformamide; DMSO, (methylsulfinyl)methane; DPPH, di-(phenyl)-(2,4,6-trinitrophenyl)iminoazanium; DTNB, 5,5′-dithiobis-2-nitrobenzoic acid; EDTA, 2,2′,2″,2‴-(ethane-1,2-diylbis(azanetriyl))tetraacetic acid; ET, electron transfer; FCS, fetal calf serum; HAT, hydrogen atom transfer; HBTU, 3-[bis(dimethylamino)methyliumyl]-3*H*-benzotriazol-1-oxide hexafluorophosphate; HPLC, high-performance liquid chromatography; ICV, intracerebroventricular; IP, intraperitoneal; MeOH, methanol; MTDL, multitarget directed ligand; MTT, 3-(4,5-dimethylthiazol-2-yl)-2,5-diphenyltetrazolium bromide; NEt_3, triethylamine; NMR, nuclear magnetic resonance; ORAC, oxygen radical absorbance capacity; PBS, phosphate buffered saline; ROS, reactive oxygen species; SDS, sodium dodecyl sulfate; Ser, serine; SI, selectivity index; ST-PA, step-through passive avoidance; TFA2, 2,2-trifluoracetic acid; UV, ultraviolet; YMT, Y-maze test

REFERENCES

(1) Alzheimer's Disease International. *World Alzheimer Report 2019: Attitudes to Dementia*; ADI: London, 2019; pp 1−168.

(2) Zemek, F.; Drtinova, L.; Nepovimova, E.; Sepsova, V.; Korabecny, J.; Klimes, J.; Kuca, K. Outcomes of Alzheimer's disease therapy with acetylcholinesterase inhibitors and memantine. *Expert Opin. Drug Saf.* **2014**, *13* (6), 759−774.

(3) Hasselmo, M. E. The role of acetylcholine in learning and memory. *Curr. Opin. Neurobiol.* **2006**, *16* (6), 710−715.

(4) Tune, L. E.; Egeli, S. Acetylcholine and delirium. *Dementia Geriatr. Cognit. Disord.* **1999**, *10* (5), 342−344.

(5) Davies, P.; Maloney, A. Selective loss of central cholinergic neurons in Alzheimer's disease. *Lancet* **1976**, *308*, 1403.

(6) Blanco-Silvente, L.; Castells, X.; Saez, M.; Barceló, M. A.; Garre-Olmo, J.; Vilalta-Franch, J.; Capellà, D. Discontinuation, efficacy, and safety of cholinesterase inhibitors for Alzheimer's disease: a meta-analysis and meta-regression of 43 randomized clinical trials enrolling 16 106 patients. *Int. J. Neuropsychopharmacol.* **2017**, *20* (7), 519−528.

(7) Arendt, T.; Brückner, M. K.; Lange, M.; Bigl, V. Changes in acetylcholinesterase and butyrylcholinesterase in Alzheimer's disease resemble embryonic development—a study of molecular forms. *Neurochem. Int.* **1992**, *21* (3), 381−396.

(8) Rao, A. A.; Sridhar, G. R.; Das, U. N. Elevated butyrylcholinesterase and acetylcholinesterase may predict the development of type 2 diabetes mellitus and Alzheimer's disease. *Med. Hypotheses* **2007**, *69* (6), 1272−1276.

(9) Campanari, M.-L.; Navarrete, F.; Ginsberg, S. D.; Manzanares, J.; Sáez-Valero, J.; García-Ayllón, M.-S. Increased expression of read-through acetylcholinesterase variants in the brains of Alzheimer's disease patients. *J. Alzheimer's Dis.* **2016**, *53* (3), 831−841.

(10) Mesulam, M. M.; Guillozet, A.; Shaw, P.; Levey, A.; Duysen, E.; Lockridge, O. Acetylcholinesterase knockouts establish central cholinergic pathways and can use butyrylcholinesterase to hydrolyze acetylcholine. *Neuroscience* **2002**, *110* (4), 627−639.

(11) Hoffmann, M.; Stiller, C.; Endres, E.; Scheiner, M.; Gunesch, S.; Sotriffer, C.; Maurice, T.; Decker, M. Highly Selective Butyrylcholinesterase Inhibitors with Tunable Duration of Action by Chemical Modification of Transferable Carbamate Units Exhibit Pronounced Neuroprotective Effect in an Alzheimer's Disease Mouse Model. *J. Med. Chem.* **2019**, *62* (20), 9116−9140.

(12) Maurice, T.; Strehaiano, M.; Siméon, N.; Bertrand, C.; Chatonnet, A. Learning performances and vulnerability to amyloid toxicity in the butyrylcholinesterase knockout mouse. *Behav. Brain Res.* **2016**, *296*, 351−360.

(13) Košak, U.; Brus, B.; Knez, D.; Šink, R.; Žakelj, S.; Trontelj, J.; Pišlar, A.; Šlenc, J.; Gobec, M.; Živin, M. Development of an in-vivo active reversible butyrylcholinesterase inhibitor. *Sci. Rep.* **2016**, *6* (1), 39495.

(14) Greig, N. H.; Utsuki, T.; Ingram, D. K.; Wang, Y.; Pepeu, G.; Scali, C.; Yu, Q.-S.; Mamczarz, J.; Holloway, H. W.; Giordano, T.; et al. Selective butyrylcholinesterase inhibition elevates brain acetylcholine, augments learning and lowers Alzheimer β-amyloid peptide in rodent. *Proc. Natl. Acad. Sci. U. S. A.* **2005**, *102* (47), 17213−17218.

(15) Cummings, J. L.; Morstorf, T.; Zhong, K. Alzheimer's disease drug-development pipeline: few candidates, frequent failures. *Alzheimer's Res. Ther.* **2014**, *6* (4), 37.

(16) Bajda, M.; Guzior, N.; Ignasik, M.; Malawska, B. Multi-target-directed ligands in Alzheimer's disease treatment. *Curr. Med. Chem.* **2011**, *18* (32), 4949−4975.

(17) Rodriguez-Soacha, D. A.; Scheiner, M.; Decker, M. Multi-target-directed-ligands acting as enzyme inhibitors and receptor ligands. *Eur. J. Med. Chem.* **2019**, *180*, 690−706.

(18) Yang, T.; Sui, X.; Yu, B.; Shen, Y.; Cong, H. Recent Advances in The Rational Drug Design Based on Multi-target Ligands. *Curr. Med. Chem.* **2020**, *27*, 4720.

(19) Wang, X.; Sun, G.; Feng, T.; Zhang, J.; Huang, X.; Wang, T.; Xie, Z.; Chu, X.; Yang, J.; Wang, H.; Chang, S.; Gong, Y.; Ruan, L.; Zhang, G.; Yan, S.; Lian, W.; Du, C.; Yang, D.; Zhang, Q.; Lin, F.; Liu, J.; Zhang, H.; Ge, C.; Xiao, S.; Ding, J.; Geng, M. Sodium oligomannate therapeutically remodels gut microbiota and suppresses gut bacterial amino acids-shaped neuroinflammation to inhibit Alzheimer's disease progression. *Cell Res.* **2019**, *29* (10), 787−803.

(20) Heneka, M. T.; Carson, M. J.; El Khoury, J.; Landreth, G. E.; Brosseron, F.; Feinstein, D. L.; Jacobs, A. H.; Wyss-Coray, T.; Vitorica, J.; Ransohoff, R. M.; Herrup, K.; Frautschy, S. A.; Finsen, B.; Brown, C. G.; Verkhratsky, A.; Yamanaka, K.; Koistinaho, J.; Latz, E.; Halle, A.; Petzold, G. C.; Town, T.; Morgan, D.; Shinohara, M. L.; Perry, V. H.; Holmes, C.; Bazan, N. G.; Brooks, D. J.; Hunot, S.; Joseph, B.; Deigendesch, N.; Garaschuk, O.; Boddeke, E.; Dinarello, C. A.; Breitner, J. C.; Cole, G. M.; Golenbock, D. T.; Kummer, M. P. Neuroinflammation in Alzheimer's disease. *Lancet Neurol.* **2015**, *14* (4), 388−405.

(21) Wang, W.-Y.; Tan, M.-S.; Yu, J.-T.; Tan, L. Role of pro-inflammatory cytokines released from microglia in Alzheimer's disease. *Ann. Transl. Med.* **2015**, *3* (10), 136.

(22) Markesbery, W. R. Oxidative stress hypothesis in Alzheimer's disease. *Free Radical Biol. Med.* **1997**, *23* (1), 134−147.

(23) Cheignon, C.; Tomas, M.; Bonnefont-Rousselot, D.; Faller, P.; Hureau, C.; Collin, F. Oxidative stress and the amyloid beta peptide in Alzheimer's disease. *Redox Biol.* **2018**, *14*, 450−464.

(24) Sawatzky, E.; Wehle, S.; Kling, B.; Wendrich, J.; Bringmann, G.; Sotriffer, C. A.; Heilmann, J.; Decker, M. Discovery of highly selective and nanomolar carbamate-based butyrylcholinesterase inhibitors by rational investigation into their inhibition mode. *J. Med. Chem.* **2016**, *59* (5), 2067−2082.

(25) Darras, F. H.; Kling, B.; Heilmann, J.; Decker, M. Neuroprotective tri-and tetracyclic BChE inhibitors releasing reversible inhibitors upon carbamate transfer. *ACS Med. Chem. Lett.* **2012**, *3* (11), 914−919.

(26) Dolles, D. Dual-acting compounds acting as receptor ligands and enzyme inhibitors. In *Design of Hybrid Molecules for Drug Development*; Decker, M., Ed. Elsevier: Amsterdam, 2017; pp 137−165.

(27) Verheijen, J. C.; Wiig, K. A.; Du, S.; Connors, S. L.; Martin, A. N.; Ferreira, J. P.; Slepnev, V. I.; Kochendörfer, U. Novel carbamate cholinesterase inhibitors that release biologically active amines following enzyme inhibition. *Bioorg. Med. Chem. Lett.* **2009**, *19* (12), 3243−3246.

(28) Toublet, F.-X.; Lalut, J.; Hatat, B.; Lecoutey, C.; Davis, A.; Since, M.; Corvaisier, S.; Freret, T.; Sopková-de Oliveira Santos, J.; Claeysen, S.; Boulouard, M.; Dallemagne, P.; Rochais, C. Pleiotropic prodrugs: Design of a dual butyrylcholinesterase inhibitor and 5-HT 6 receptor antagonist with therapeutic interest in Alzheimer's disease. *Eur. J. Med. Chem.* **2021**, *210*, 113059.

https://doi.org/10.1021/acs.jmedchem.1c00534
J. Med. Chem. 2021, 64, 9302−9320

(29) Zussy, C.; Brureau, A.; Delair, B.; Marchal, S.; Keller, E.; Ixart, G.; Naert, G.; Meunier, J.; Chevallier, N.; Maurice, T.; Givalois, L. Time-course and regional analyses of the physiopathological changes induced after cerebral injection of an amyloid β fragment in rats. *Am. J. Pathol.* **2011**, *179* (1), 315−334.
(30) Knez, D.; Coquelle, N.; Pišlar, A.; Žakelj, S.; Jukič, M.; Sova, M.; Mravljak, J.; Nachon, F.; Brazzolotto, X.; Kos, J.; Colletier, J. P.; Gobec, S. Multi-target-directed ligands for treating Alzheimer's disease: butyrylcholinesterase inhibitors displaying antioxidant and neuroprotective activities. *Eur. J. Med. Chem.* **2018**, *156*, 598−617.
(31) Benchekroun, M.; Romero, A.; Egea, J.; Leon, R.; Michalska, P.; Buendía, I.; Jimeno, M. L.; Jun, D.; Janockova, J.; Sepsova, V.; Soukup, O.; Bautista-Aguilera, O. M.; Refouvelet, B.; Ouari, O.; Marco-Contelles, J.; Ismaili, L. The antioxidant additive approach for Alzheimer's disease therapy: new ferulic (lipoic) acid plus melatonin modified tacrines as cholinesterases inhibitors, direct antioxidants, and nuclear factor (erythroid-derived 2)-like 2 activators. *J. Med. Chem.* **2016**, *59* (21), 9967−9973.
(32) Wang, J.; Wang, Z.-M.; Li, X.-M.; Li, F.; Wu, J.-J.; Kong, L.-Y.; Wang, X.-B. Synthesis and evaluation of multi-target-directed ligands for the treatment of Alzheimer's disease based on the fusion of donepezil and melatonin. *Bioorg. Med. Chem.* **2016**, *24* (18), 4324−4338.
(33) Darvesh, S.; Hopkins, D. A.; Geula, C. Neurobiology of butyrylcholinesterase. *Nat. Rev. Neurosci.* **2003**, *4* (2), 131−138.
(34) Mesulam, M.; Geula, C. Butyrylcholinesterase reactivity differentiates the amyloid plaques of aging from those of dementia. *Ann. Neurol.* **1994**, *36* (5), 722−727.
(35) Guillozet, A.; Mesulam, M. M.; Smiley, J.; Mash, D. Butyrylcholinesterase in the life cycle of amyloid plaques. *Ann. Neurol.* **1997**, *42* (6), 909−918.
(36) Simunkova, M.; Alwasel, S. H.; Alhazza, I. M.; Jomova, K.; Kollar, V.; Rusko, M.; Valko, M. Management of oxidative stress and other pathologies in Alzheimer's disease. *Arch. Toxicol.* **2019**, *93* (93), 2491−2513.
(37) Schramm, S.; Huang, G.; Gunesch, S.; Lang, F.; Roa, J.; Högger, P.; Sabaté, R.; Maher, P.; Decker, M. Regioselective synthesis of 7-O-esters of the flavonolignan silibinin and SARs lead to compounds with overadditive neuroprotective effects. *Eur. J. Med. Chem.* **2018**, *146*, 93−107.
(38) Spuch, C.; Antequera, D.; Isabel Fernandez-Bachiller, M.; Isabel Rodríguez-Franco, M.; Carro, E. A new tacrine-melatonin hybrid reduces amyloid burden and behavioral deficits in a mouse model of Alzheimer's disease. *Neurotoxic. Res.* **2010**, *17* (4), 421−431.
(39) Mihardja, M.; Roy, J.; Wong, K. Y.; Aquili, L.; Heng, B. C.; Chan, Y. S.; Fung, M. L.; Lim, L. W. Therapeutic potential of neurogenesis and melatonin regulation in Alzheimer's disease. *Ann. N. Y. Acad. Sci.* **2020**, *1478* (1), 43−62.
(40) Fang, L.; Kraus, B.; Lehmann, J.; Heilmann, J.; Zhang, Y.; Decker, M. Design and synthesis of tacrine-ferulic acid hybrids as multi-potent anti-Alzheimer drug candidates. *Bioorg. Med. Chem. Lett.* **2008**, *18* (9), 2905−2909.
(41) Lan, J.-S.; Zeng, R.-F.; Jiang, X.-Y.; Hou, J.-W.; Liu, Y.; Hu, Z.-H.; Li, H.-X.; Li, Y.; Xie, S.-S.; Ding, Y.; Zhang, T. Design, synthesis and evaluation of novel ferulic acid derivatives as multi-target-directed ligands for the treatment of Alzheimer's disease. *Bioorg. Chem.* **2020**, *94*, 103413.
(42) Gunesch, S.; Hoffmann, M.; Kiermeier, C.; Fischer, W.; Pinto, A. F.; Maurice, T.; Maher, P.; Decker, M. 7-O-Esters of taxifolin with pronounced and overadditive effects in neuroprotection, anti-neuroinflammation, and amelioration of short-term memory impairment in vivo. *Redox Biol.* **2020**, *29*, 101378.
(43) Peperidou, A.; Pontiki, E.; Hadjipavlou-Litina, D.; Voulgari, E.; Avgoustakis, K. Multifunctional cinnamic acid derivatives. *Molecules* **2017**, *22* (8), 1247.
(44) Cai, P.; Fang, S.-Q.; Yang, X.-L.; Wu, J.-J.; Liu, Q.-H.; Hong, H.; Wang, X.-B.; Kong, L.-Y. Rational design and multibiological profiling of novel donepezil-trolox hybrids against Alzheimer's disease, with cholinergic, antioxidant, neuroprotective, and cognition enhancing properties. *ACS Chem. Neurosci.* **2017**, *8* (11), 2496−2511.
(45) Nepovimova, E.; Korabecny, J.; Dolezal, R.; Babkova, K.; Ondrejicek, A.; Jun, D.; Sepsova, V.; Horova, A.; Hrabinova, M.; Soukup, O.; et al. Tacrine-trolox hybrids: a novel class of centrally active, nonhepatotoxic multi-target-directed ligands exerting anticholinesterase and antioxidant activities with low in vivo toxicity. *J. Med. Chem.* **2015**, *58* (22), 8985−9003.
(46) Sawatzky, E.; Al-Momani, E.; Kobayashi, R.; Higuchi, T.; Samnick, S.; Decker, M. A novel way to radiolabel human butyrylcholinesterase for positron emission tomography through irreversible transfer of the radiolabeled moiety. *ChemMedChem* **2016**, *11* (14), 1540−1550.
(47) Sawatzky, E.; Bukowczan, J.; Decker, M. Investigation into selective debenzylation and ring cleavage of quinazoline based heterocycles. *Tetrahedron Lett.* **2014**, *55* (18), 2973−2976.
(48) Ellman, G. L. A colorimetric method for determining low concentrations of mercaptans. *Arch. Biochem. Biophys.* **1958**, *74* (2), 443−450.
(49) Ellman, G. L.; Courtney, K. D.; Andres, V., Jr; Featherstone, R. M. A new and rapid colorimetric determination of acetylcholinesterase activity. *Biochem. Pharmacol.* **1961**, *7* (2), 88−95.
(50) Montanari, S.; Scalvini, L.; Bartolini, M.; Belluti, F.; Gobbi, S.; Andrisano, V.; Ligresti, A.; Di Marzo, V.; Rivara, S.; Mor, M.; et al. Fatty acid amide hydrolase (FAAH), acetylcholinesterase (AChE), and butyrylcholinesterase (BuChE): networked targets for the development of carbamates as potential anti-Alzheimer's disease agents. *J. Med. Chem.* **2016**, *59* (13), 6387−6406.
(51) Prior, R. L.; Wu, X.; Schaich, K. Standardized methods for the determination of antioxidant capacity and phenolics in foods and dietary supplements. *J. Agric. Food Chem.* **2005**, *53* (10), 4290−4302.
(52) Fulgenzi, A.; Ferrero, M. E. EDTA chelation therapy for the treatment of neurotoxicity. *Int. J. Mol. Sci.* **2019**, *20* (5), 1019.
(53) Davis, J. B.; Maher, P. Protein kinase C activation inhibits glutamate-induced cytotoxicity in a neuronal cell line. *Brain Res.* **1994**, *652* (1), 169−173.
(54) Murphy, T. H.; Miyamoto, M.; Sastre, A.; Schnaar, R. L.; Coyle, J. T. Glutamate toxicity in a neuronal cell line involves inhibition of cystine transport leading to oxidative stress. *Neuron* **1989**, *2* (6), 1547−1558.
(55) Tan, S.; Wood, M.; Maher, P. Oxidative stress induces a form of programmed cell death with characteristics of both apoptosis and necrosis in neuronal cells. *J. Neurochem.* **1998**, *71* (1), 95−105.
(56) Tan, S.; Schubert, D.; Maher, P. Oxytosis: a novel form of programmed cell death. *Curr. Top. Med. Chem.* **2001**, *1* (6), 497−506.
(57) Schramm, S.; Gunesch, S.; Lang, F.; Saedtler, M.; Meinel, L.; Högger, P.; Decker, M. Investigations into neuroprotectivity, stability, and water solubility of 7-O-cinnamoylsilibinin, its hemisuccinate and dehydro derivatives. *Arch. Pharm.* **2018**, *351* (11), 1800206.
(58) Scheiner, M.; Dolles, D.; Gunesch, S.; Hoffmann, M.; Nabissi, M.; Marinelli, O.; Naldi, M.; Bartolini, M.; Petralla, S.; Poeta, E.; Monti, B.; Falkeis, C.; Vieth, M.; Hübner, H.; Gmeiner, P.; Maitra, R.; Maurice, T.; Decker, M. Dual-Acting Cholinesterase-Human Cannabinoid Receptor 2 Ligands Show Pronounced Neuroprotection in Vitro and Overadditive and Disease-Modifying Neuroprotective Effects in Vivo. *J. Med. Chem.* **2019**, *62* (20), 9078−9102.
(59) Maurice, T.; Lockhart, B. P.; Privat, A. Amnesia induced in mice by centrally administered β-amyloid peptides involves cholinergic dysfunction. *Brain Res.* **1996**, *706* (2), 181−193.
(60) Lahmy, V.; Meunier, J.; Malmström, S.; Naert, G.; Givalois, L.; Kim, S. H.; Villard, V.; Vamvakides, A.; Maurice, T. Blockade of Tau hyperphosphorylation and Aβ 1−42 generation by the aminotetrahydrofuran derivative ANAVEX2−73, a mixed muscarinic and σ 1 receptor agonist, in a nontransgenic mouse model of Alzheimer's disease. *Neuropsychopharmacology* **2013**, *38* (9), 1706−1723.
(61) Wade, A. G.; Farmer, M.; Harari, G.; Fund, N.; Laudon, M.; Nir, T.; Frydman-Marom, A.; Zisapel, N. Add-on prolonged-release melatonin for cognitive function and sleep in mild to moderate

https://doi.org/10.1021/acs.jmedchem.1c00534
J. Med. Chem. 2021, 64, 9302−9320

Alzheimer's disease: a 6-month, randomized, placebo-controlled, multicenter trial. *Clin. Interv. Aging* **2014**, *9*, 947.
(62) U.S. National Library of Medicine. Bisnorcymserine in Healthy Adult Volunteers. *ClinicalTrials.gov*, 2012. https://clinicaltrials.gov/ct2/show/NCT01747213 (accessed 2020-02-03).
(63) U.S. National Library of Medicine. Disease Modifying Potential of 5mg of Melatonin on Cognition and Brain Health in Aging. *ClinicalTrials.gov*, 2019. https://clinicaltrials.gov/ct2/show/NCT03954899?term=Melatonin&cond=Alzheimer+Disease&draw=2&rank=3 (accessed 2020-02-17).
(64) Sharma, O. P.; Bhat, T. K. DPPH antioxidant assay revisited. *Food Chem.* **2009**, *113* (4), 1202−1205.
(65) Ou, B.; Hampsch-Woodill, M.; Prior, R. L. Development and validation of an improved oxygen radical absorbance capacity assay using fluorescein as the fluorescent probe. *J. Agric. Food Chem.* **2001**, *49* (10), 4619−4626.
(66) Dávalos, A.; Gómez-Cordovés, C.; Bartolomé, B. Extending applicability of the oxygen radical absorbance capacity (ORAC-fluorescein) assay. *J. Agric. Food Chem.* **2004**, *52* (1), 48−54.
(67) Santos, J. S.; Alvarenga Brizola, V. R.; Granato, D. High-throughput assay comparison and standardization for metal chelating capacity screening: A proposal and application. *Food Chem.* **2017**, *214*, 515−522.
(68) Li, B.; Duysen, E. G.; Lockridge, O. The butyrylcholinesterase knockout mouse is obese on a high-fat diet. *Chem.-Biol. Interact.* **2008**, *175* (1−3), 88−91.
(69) Maurice, T.; Su, T.-P.; Privat, A. Sigma$_1$ (σ_1) receptor agonists and neurosteroids attenuate β_{25-35}-amyloid peptide-induced amnesia in mice through a common mechanism. *Neuroscience* **1998**, *83*, 413−428.
(70) Meunier, J.; Ieni, J.; Maurice, T. The anti-amnesic and neuroprotective effects of donepezil against amyloid β_{25-35} peptide-induced toxicity in mice involve an interaction with the σ_1 receptor. *Br. J. Pharmacol.* **2006**, *149*, 998−1012.
(71) Meunier, J.; Villard, V.; Givalois, L.; Maurice, T. The γ-secretase inhibitor 2-[(1R)-1-[(4-chlorophenyl)sulfonyl](2,5-difluorophenyl) amino]ethyl-5-fluorobenzenebutanoic acid (BMS-299897) alleviates Aβ_{1-42} seeding and short-term memory deficits in the Aβ_{25-35} mouse model of Alzheimer's disease. *Eur. J. Pharmacol.* **2013**, *698*, 193−199.
(72) Villard, V.; Espallergues, J.; Keller, E.; Alkam, T.; Nitta, A.; Yamada, K.; Nabeshima, T.; Vamvakides, A.; Maurice, T. Antiamnesic and Neuroprotective Effects of the Aminotetrahydrofuran Derivative ANAVEX1-41 Against Amyloid β_{25-35}-Induced Toxicity in Mice. *Neuropsychopharmacology* **2009**, *34*, 1552−1566.
(73) Villard, V.; Espallergues, J.; Keller, E.; Vamvakides, A.; Maurice, T. Anti-amnesic and neuroprotective potentials of the mixed muscarinic receptor/sigma1 (σ1) ligand ANAVEX2-73, a novel aminotetrahydrofuran derivative. *J. Psychopharmacol.* **2011**, *25*, 1101−1117.

https://doi.org/10.1021/acs.jmedchem.1c00534
J. Med. Chem. 2021, 64, 9302−9320